

# Toward a Mølmer Sørensen Gate With .9999 Fidelity

Reinhold Blümel

*Wesleyan University, Middletown, CT 06459, USA and*

*IonQ, College Park, MD 20740, USA*

Andrii Maksymov and Ming Li

*IonQ, College Park, MD 20740, USA*

(Dated: November 28, 2023)

## Abstract

Realistic fault-tolerant quantum computing at reasonable overhead requires two-qubit gates with the highest possible fidelity. Typically, an infidelity of  $\lesssim 10^{-4}$  is recommended in the literature. Focusing on the phase-sensitive architecture used in laboratories and by commercial companies to implement quantum computers, we show that even under noise-free, ideal conditions, neglecting the carrier term and linearizing the Lamb-Dicke term in the Hamiltonian used for control-pulse construction for generating Mølmer-Sørensen XX gates based on the Raman scheme are not justified if the goal is an infidelity target of  $10^{-4}$ . We obtain these results with a gate simulator code that, in addition to the computational space, explicitly takes the most relevant part of the phonon space into account. With the help of a Magnus expansion carried to the third order, keeping terms up to the fourth order in the Lamb-Dicke parameters, we identify the leading sources of coherent errors, which we show can be eliminated by adding a single linear equation to the phase-space closure conditions and subsequently adjusting the amplitude of the control pulse (calibration). This way, we obtain XX gates with infidelities  $< 10^{-4}$ .

## I. INTRODUCTION

The trapped-ion architecture, i.e., chains of trapped ions, coherently controlled via Raman hyperfine transitions, is one of the most promising routes to scalable quantum computing [1–10]. This quantum computer architecture is used both in laboratory experiments and in the emerging quantum computing industry [7–11]. For both the current era of noisy intermediate-scale quantum computing [12] and the anticipated era of fault-tolerant, error-corrected quantum computing [1], two-qubit gates of the highest possible fidelity are essential. While fault-tolerant quantum computing and quantum error-correction may, in principle, be achieved with two-qubit gates of modest fidelity, the overhead, i.e., the number of physical qubits required for one error-corrected logical qubit depends on the native fidelity of the physical gates and may be enormous for physical two-qubit gates of only modest fidelity. A reasonable amount of overhead in fault-tolerant quantum computing can be achieved only if the physical two-qubit gates themselves have a high native fidelity. Typically, for realistic, tolerable overhead, a physical two-qubit infidelity of  $\lesssim 10^{-4}$  is recommended [12–15]. Two-qubit gate infidelities close to this target have indeed already been achieved [16–18]. However, the experimental demonstrations of high-fidelity two-qubit gates are restricted to two-qubit gates in very short ion chains, i.e., chains consisting of up to four ions. Moreover, to date, even in these cases two-qubit gate infidelities of  $\lesssim 10^{-4}$  have not yet been achieved experimentally. Two adversaries stand in the way of achieving two-qubit gate infidelities  $\lesssim 10^{-4}$ : Random noise and deterministic, coherent control errors. Even in the shortest chains (two to four ions stored simultaneously), the target of  $\lesssim 10^{-4}$  infidelity may not be achieved if the Hamiltonian used to design the control pulses for two-qubit gate implementation does not accurately enough reflect the reality of the quantum computer’s hardware implementation. What this means is illustrated in Fig. 1. The actual quantum computer, i.e., the reality, is governed by a Hamiltonian  $\hat{H}_R$ . Reality can never be captured exactly. It can only be modeled approximately. Consequently a model of the quantum computer is constructed (see Section II), replacing the unknown Hamiltonian  $\hat{H}_R$  with  $\hat{H}_M$ , where it is hoped that  $\hat{H}_M \sim \hat{H}_R$  to a high accuracy. Both the quantum computer ( $\hat{H}_R$ ) and its model ( $\hat{H}_M$ ) are controlled by control pulses that are constructed on the basis of a Hamiltonian  $\hat{H}_C$ . Ideally,  $\hat{H}_C = \hat{H}_R$ . However, since  $\hat{H}_R$  is unknown, the best possible control Hamiltonian is  $\hat{H}_C = \hat{H}_M$ . However, in most cases  $\hat{H}_M$  is too complicated to use for

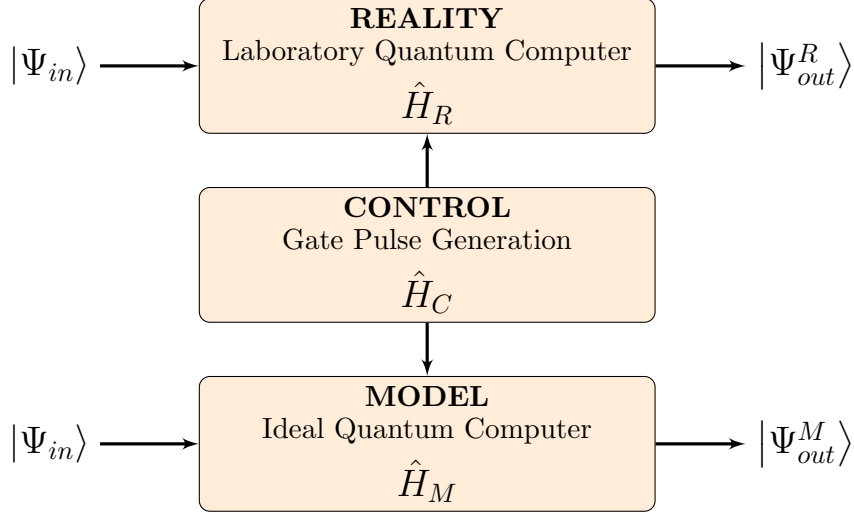


FIG. 1. Relationship between a hardware-implemented quantum computer (REALITY, governed by the Hamiltonian  $\hat{H}_R$ ), the corresponding model quantum computer (MODEL, governed by the model Hamiltonian  $\hat{H}_M$ ) and the control pulses (CONTROL, constructed on the basis of the control Hamiltonian  $\hat{H}_C$ ) that control both the actual hardware-implemented quantum computer (REALITY) and the model quantum computer (MODEL). Although controlled by the same control pulse, since  $\hat{H}_M$  is close to, but not equal to  $\hat{H}_R$ , a given input state  $|\psi_{in}\rangle$  results in two different output states  $|\psi_{out}^R\rangle \neq |\psi_{out}^M\rangle$ , which depend on whether  $|\psi_{in}\rangle$  is processed by  $\hat{H}_R$  or  $\hat{H}_M$ , respectively. The overlap  $|\langle\psi_M|\psi_R\rangle|^2$ , then, is a measure of how close  $\hat{H}_M$  is to  $\hat{H}_R$ .

efficiently constructing control pulses that frequently also have to be computed in real time. Therefore,  $\hat{H}_C$  is chosen as a compromise, close enough to  $\hat{H}_M$  to ensure acceptable control of the quantum computer, but simple enough to ensure efficient control-pulse construction.

One of the most basic tasks of a quantum computer is to construct two-qubit gates [1]. In this paper, we focus on two-qubit XX gates constructed according to the Mølmer-Sørensen scheme [19–21]. Ideally, given an input state,  $|\psi_{in}\rangle$ , the quantum computer, governed by  $\hat{H}_R$ , is expected to turn  $|\psi_{in}\rangle$  into  $|\psi_{out}\rangle = XX|\psi_{in}\rangle$ , where XX is the ideal XX gate [1]. However, since  $\hat{H}_R \neq \hat{H}_C$ , this will not happen in practice. Therefore,  $|\psi_{out}^R\rangle$ , i.e., the output state produced by  $\hat{H}_R$ , is different from  $XX|\psi_{in}\rangle$ . How different, and given the absence of knowledge of  $\hat{H}_R$ , can only be answered by experimental quantum-state tomography [22] and is beyond the scope of this paper. However, assuming that  $\hat{H}_M$  is very close to  $\hat{H}_R$ , it

is possible, at least approximately, to assess the quality of the control pulses by computing the model output state  $|\psi_{\text{out}}^{\text{M}}\rangle$  and comparing it with the ideal output state  $XX|\psi_{\text{in}}\rangle$ , for instance, by computing the overlap  $|\langle\psi_{\text{out}}^{\text{M}}|XX|\psi_{\text{in}}\rangle|^2$ . Only for  $\hat{H}_C = \hat{H}_M$  do we expect this overlap to equal 1. However, if  $\hat{H}_M$  is close to  $\hat{H}_R$ , but  $\hat{H}_C$  is chosen as the manageable standard Hamiltonian  $\hat{H}_S$  (see Section II), we expect this overlap and other fidelity measures (see Section V) to differ from 1. In this case, because of the insufficient quality of the control pulses, the resulting two-qubit gates may not be accurate enough for the target infidelity (for instance,  $< 10^{-4}$ ). To assess this difference, and to develop an  $\hat{H}_C$  that produces an infidelity  $\lesssim 10^{-4}$  is the purpose of this paper. To this end, constructing a realistic model Hamiltonian  $\hat{H}_M$  for Raman-controlled trapped ions, we show in this paper that currently employed control-pulse construction techniques based the standard Hamiltonian  $\hat{H}_S$ , i.e.,  $\hat{H}_C = \hat{H}_S$  (see, e.g., [23]) are not accurate enough to achieve the  $\lesssim 10^{-4}$  infidelity target for realistic fault-tolerant quantum computing. We show this by constructing control pulses on the basis of  $\hat{H}_S$ , which we then use to compute two-qubit XX gates in a 7-ion chain governed by  $\hat{H}_M$ , assuming that  $\hat{H}_M$  is sufficiently close to  $\hat{H}_R$ . The XX gate simulations of the 7-ion chain are performed with a gate-simulator code that is accurate on the  $10^{-7}$  level and takes both computational levels and phonon states explicitly into account. This way we show that even assuming ideal conditions, i.e., neglecting all incoherent noise sources, control-pulse construction needs to be improved to reach the  $\lesssim 10^{-4}$  infidelity goal.

There are two principal methods of implementing a trapped-ion chain quantum computer using the stimulated Raman scheme: Phase sensitive and phase insensitive [24]. Both schemes have advantages and disadvantages. While errors in the phase-insensitive scheme were studied before in detail [24], we focus in this paper on the phase-sensitive scheme since it is technically more straightforward to implement and is currently used by commercial quantum computing companies such as IonQ. Therefore, the focus in this paper is to isolate the leading coherent error sources in the phase-sensitive architecture and to construct methods that allow us to eliminate these error sources. We show in this paper that on the basis of a new *linear* scheme of pulse construction, and in the absence of all incoherent error sources, we reach XX gate infidelities  $\lesssim 10^{-4}$ .

Our paper is organized as follows. We start in Section II by presenting various Hamiltonians used in gate construction and error analysis. In Section III we discuss pulse construction methods, focusing on the AMFM pulse-construction method [23] that we are using through-

out this paper for generating test pulses. In Section IV we present our gate-simulation method that propagates an initial state  $|\psi(t=0)\rangle$  into a final state  $|\psi(\tau)\rangle$ , where  $\tau$  is the gate time, including the 2-qubit computational space and a portion of the phonon space large enough to obtain converged results. In Section V we define various fidelity measures that we use to assess the quality of various Hamiltonians used to construct XX gates. In Section VI we present our numerical simulation results. In Section VII we present a simple pulse-scaling method (calibration) that may be used to eliminate coherent errors that result in XX gates that deviate from the target degree of entanglement. In Section VIII we analyze sources of errors that are incurred by using a pulse function  $g(t)$  constructed on the basis of the standard Hamiltonian to control a quantum computer assumed to be governed by the full Mølmer-Sørensen Hamiltonian. The analysis is conducted analytically and error integrals are evaluated numerically to assess error magnitudes. In Section IX we present our *linear* method of eliminating an important class of coherent errors. It is this method, together with pulse calibration that allows us to suppress coherent XX gate errors to the level of  $\lesssim 10^{-4}$ . In Section X we investigate the scaling of our results to the case of chains consisting of 32 ions. In Section XI we discuss our results. In Section XII we present a brief summary of our results and conclude the paper.

## II. HAMILTONIAN

In this section we derive the model Hamiltonian  $\hat{H}_M$ , which we take to be the full Mølmer-Sørensen Hamiltonian that governs a chain of ions in a linear Paul trap [11], illuminated simultaneously by two laser beams, one red detuned and one blue detuned [19, 20]. The derivation starts with the effective two-level Hamiltonian [25]

$$\hat{H} = \hat{H}_0 + \sum_{j=1}^N \left( \frac{\hbar\Omega_{\text{eff}}(t)}{2} \right) e^{-i[(\Delta\vec{k})\cdot\vec{r}_j - \mu t - \Delta\varphi]} \hat{\sigma}_-^{(j)} + h.c., \quad (1)$$

obtained via adiabatic elimination according to the Raman  $\Lambda$  scheme [24]. Here,  $N$  is the number of ions in the chain,

$$\hat{H}_0 = \sum_{p=1}^N \hbar\omega_p \hat{a}_p^\dagger \hat{a}_p \quad (2)$$

is the phonon Hamiltonian with the phonon frequencies  $\omega_p$  and associated phonon creation and destruction operators  $\hat{a}_p^\dagger$  and  $\hat{a}_p$ , respectively, the  $j$  sum is over the ions in the chain,

$\Omega_{\text{eff}}(t)$  is the time-dependent effective Rabi frequency,  $\Delta\vec{k}$  is the wavenumber difference between the two Raman lasers,  $\vec{r}_j$  is the position operator of ion number  $j$  in the chain, and  $\Delta\varphi$  is the phase difference between the two Raman lasers.

To construct a Mølmer-Sørensen (MS) gate [19, 20, 25], we illuminate the ions simultaneously with blue ( $+\mu$ ) and red ( $-\mu$ ) shifted light and, after moving to the interaction representation with respect to  $\hat{H}_0$ , we obtain the MS Hamiltonian

$$\begin{aligned} \hat{H}_{\text{MS}}(t) = \sum_j \hbar\Omega_j \cos(\mu t - \phi_j^m) & \left\{ \cos \left[ \sum_p \eta_p^j (\hat{a}_p^\dagger e^{i\omega_p t} + \hat{a}_p e^{-i\omega_p t}) \right] \hat{\sigma}_y^{(j)} \right. \\ & \left. + \sin \left[ \sum_p \eta_p^j (\hat{a}_p^\dagger e^{i\omega_p t} + \hat{a}_p e^{-i\omega_p t}) \right] \hat{\sigma}_x^{(j)} \right\}, \end{aligned} \quad (3)$$

where  $\mu$  is the detuning frequency [11],  $\eta_p^j$  are the Lamb-Dicke parameters [11], and  $\hat{\sigma}_x$ ,  $\hat{\sigma}_y$ ,  $\hat{\sigma}_z$  are the Pauli operators. The Hamiltonian (3) may be generalized according to

$$\hbar\Omega_j \cos(\mu t - \phi_j^m) \rightarrow \hbar\Omega_j(t) \cos \left[ \int_0^t \mu(t') dt' + \phi_j^{(0)} \right] \rightarrow \hbar g_j(t), \quad (4)$$

where  $g_j(t)$  may be any time-dependent pulse function, i.e., it includes amplitude-modulated (AM) pulses [4, 26, 27], frequency-modulated (FM) pulses [28], phase-modulated (PM) pulses [29–31], and simultaneously amplitude- and frequency-modulated (AMFM) pulses [23, 32]. Thus, written in terms of the most general pulse function  $g_j(t)$ , the MS Hamiltonian (3) becomes:

$$\hat{H}_{\text{MS}} = \sum_j \hbar g_j(t) \left\{ \cos [\hat{V}_j(t)] \hat{\sigma}_y^{(j)} + \sin [\hat{V}_j(t)] \hat{\sigma}_x^{(j)} \right\}, \quad (5)$$

where, for later convenience, we defined the Lamb-Dicke operators

$$\hat{V}_j(t) = \sum_p \eta_p^j (\hat{a}_p^\dagger e^{i\omega_p t} + \hat{a}_p e^{-i\omega_p t}), \quad (6)$$

which satisfy

$$[\hat{V}_j(t_1), \hat{V}_l(t_2)] = -2i \sum_p \eta_p^j \eta_p^l \sin[\omega_p(t_1 - t_2)]. \quad (7)$$

Expanding  $\hat{H}_{\text{MS}}$  in powers of  $\hat{V}$ , we obtain a family of model Hamiltonians

$$\hat{H}_M^{(N_c, N_s)} = \sum_j \hbar g_j(t) \left\{ \sum_{\substack{n=0 \\ n \text{ even}}}^{N_c} (-1)^{n/2} \frac{\hat{\sigma}_y^{(j)}}{n!} \hat{V}_j^n(t) + \sum_{\substack{m=1 \\ m \text{ odd}}}^{N_s} (-1)^{(m-1)/2} \frac{\hat{\sigma}_x^{(j)}}{m!} \hat{V}_j^m(t) \right\}, \quad (8)$$

where

$$\hat{H}_M^{(\infty,\infty)} = \hat{H}_{MS}. \quad (9)$$

For later convenience, we also define the standard Hamiltonian

$$\hat{H}_S = \hat{H}_M^{(-2,1)} = \sum_j \hbar g_j(t) \hat{V}_j(t) \hat{\sigma}_x^{(j)}, \quad (10)$$

which is frequently used in the literature as the basis for control-pulse construction [23, 26, 28–31]. Here, the superscript  $N_c = -2$  codes for the complete suppression (omission) of the cosine term in (8). The test pulses used in this paper are also all constructed on the basis of  $\hat{H}_S$  (see Section III). The expanded model Hamiltonians (8) are used in Section VI to assess the accuracy of expansions of  $\hat{H}_{MS}$  in powers of the Lamb-Dicke operators  $\hat{V}_j(t)$ .

### III. CONTROL-PULSE CONSTRUCTION

To control  $\hat{H}_R$  and  $\hat{H}_M$  (see Fig. 1), we need a pulse function  $g(t)$  (see Section II). Several different pulse-construction schemes have been proposed in the past, including amplitude modulation [4, 26, 27], phase modulation [29–31], frequency modulation [28], and simultaneous amplitude- and frequency modulation [23, 32]. All these pulse-construction schemes have in common that they are based on the standard Hamiltonian  $\hat{H}_S$  defined in (10). For this paper we choose sine-AMFM pulses [23, 32] since they are power-optimal and straightforward to construct. They are defined as

$$g(t) = \sum_{n_{\min}}^{n_{\max}} B_n \sin(\omega_n t), \quad (11)$$

where the basis spans the states  $n \in \{n_{\min}, n_{\max}\}$ ,  $B_n$  are real amplitudes,

$$\omega_n = \frac{2\pi n}{\tau} \quad (12)$$

are the basis frequencies, and  $\tau$  is the gate time. The pulse functions (11) fulfill

$$\int_0^\tau g(t) dt = 0, \quad (13)$$

an important property assumed to hold in all of our analytical calculations.

Phase-space closure [11, 23, 32] requires

$$\alpha_p^j = -\eta_p^j \int_0^\tau g_j(t) e^{i\omega_p t} dt = 0, \quad p, j = 1, \dots, N. \quad (14)$$

The sine-AMFM pulses (11), constructed according to [23], fulfill (14) exactly. Throughout this paper we choose  $N = 7$ , i.e., we investigate the quality of two-qubit XX gates in a chain of  $N = 7$  ions.  $N = 7$  was chosen because it is large enough to be realistic [23, 32], yet small enough to enable direct numerical simulations of the quantum dynamics of the chain explicitly including a large phonon space. In addition, throughout this paper, we choose  $g_j(t) = g(t)$ ,  $j = 1, \dots, N$ , i.e., whenever we construct a two-qubit gate between two ions, we assume that each of the two ions is irradiated with laser light controlled by the same pulse function  $g(t)$ . This is a common choice, used in laboratories [23, 32] and in commercial quantum computers [3].

In addition to fulfilling the phase-space closure condition (14), the pulse  $g(t)$  has to produce the desired degree of entanglement  $\chi$  according to [23]

$$\chi = 2 \sum_{p=1}^N \eta_p^{j_1} \eta_p^{j_2} \int_0^\tau dt \int_0^t dt' g(t) g(t') \sin[\omega_p(t-t')]. \quad (15)$$

A maximally entangling gate is obtained for  $\chi = \pi/4$ . The mode frequencies  $\omega_p$ ,  $p = 1, \dots, 7$ , and the Lamb-Dicke parameters  $\eta_p^j$ ,  $p, j = 1, \dots, 7$ , are listed in Tables I and II, respectively.

For computing analytical infidelities we will make extensive use of the following identities that follow directly from (14) with the expansion (11) and hold for all  $p = 1, \dots, N$ :

$$\int_0^\tau g(t) e^{\pm i\omega_p t} dt = 0, \quad (16)$$

$$\int_0^\tau g(t) \sin(\omega_p t) dt = 0, \quad (17)$$

$$\int_0^\tau g(t) \cos(\omega_p t) dt = 0, \quad (18)$$

$$\sum_{n_{\min}}^{n_{\max}} B_n \left( \frac{\omega_n}{\omega_n^2 - \omega_p^2} \right) = 0. \quad (19)$$

For later use in the following sections, we also define

$$\tilde{\chi} = \sum_{jp} (\eta_p^j)^2 \int_0^\tau dt \int_0^t dt' g(t) g(t') \sin[\omega_p(t-t')], \quad (20)$$

$$G(t) = \int_0^t g(t') dt' = \sum_n \left( \frac{B_n}{\omega_n} \right) [1 - \cos(\omega_n t)] = 2 \sum_n \left( \frac{B_n}{\omega_n} \right) \sin^2(\omega_n t/2), \quad (21)$$

$$Q(w) = \int_0^\tau g(t) e^{iwt} dt = [e^{iw\tau} - 1] \sum_n B_n \left( \frac{\omega_n}{w^2 - \omega_n^2} \right), \quad (22)$$



$$\begin{aligned}
f(w) &= \int_0^\tau g(t)G(t)e^{iwt} dt \\
&= \left(\frac{1}{2}\right) [e^{iw\tau} - 1] \sum_{nm} \left(\frac{B_n B_m}{\omega_n}\right) \left\{ \frac{\omega_m - \omega_n}{(\omega_m - \omega_n)^2 - w^2} + \frac{\omega_m + \omega_n}{(\omega_m + \omega_n)^2 - w^2} \right\}, \quad (23)
\end{aligned}$$

$$\begin{aligned}
S_p(w) &= \int_0^\tau dt_1 \int_0^{t_1} dt_2 g(t_1)g(t_2) \sin[\omega_p(t_1 - t_2)]e^{iwt_1} \\
&= \int_0^\tau dt_1 \int_0^{t_1} dt_2 g(t_1)g(t_2) \sin[\omega_p(t_1 - t_2)]e^{iwt_2} \\
&= \sum_{nm} \frac{B_n B_m}{2(w^2 - \omega_m^2)} \left\{ \left(\frac{2\omega_n \omega_m}{\omega_n^2 - 4w^2}\right) e^{iw\tau} \sin(w\tau) \right. \\
&\quad \left. + iw^2 (e^{iw\tau} - 1) \left[ \frac{1}{(\omega_n - \omega_m)^2 - w^2} - \frac{1}{(\omega_n + \omega_m)^2 - w^2} \right] \right\}, \quad (24)
\end{aligned}$$

$$J_p = \int_0^\tau g(t)G^2(t)e^{i\omega_p t} dt, \quad (25)$$

$$\begin{aligned}
Z(w_1, w_2) &= \int_0^\tau dt_1 \int_0^{t_1} dt_2 g(t_1)g(t_2)e^{iw_1 t_1} e^{iw_2 t_2} \\
&= \sum_{nm} B_n B_m \left(\frac{1}{\omega_m^2 - w_2^2}\right) \left\{ \left(\frac{\omega_n \omega_m}{w_1^2 - \omega_n^2}\right) [e^{iw_1 \tau} - 1] \right. \\
&\quad \left. - \left(\frac{\omega_n \omega_m (\omega_m^2 - \omega_n^2 + w_1^2 + 4w_1 w_2 + 3w_2^2)}{[(\omega_n + \omega_m)^2 - (w_1 + w_2)^2][(\omega_n - \omega_m)^2 - (w_1 + w_2)^2]}\right) [e^{i(w_1 + w_2)\tau} - 1] \right\}, \quad (26)
\end{aligned}$$

and

$$\begin{aligned}
\Phi[\eta, g] &= \sum_{p=1}^N \eta_p^1 \eta_p^2 \int_0^\tau dt_1 \int_0^{t_1} dt_2 g(t_1)g(t_2)G(t_2) \sin[\omega_p(t_1 - t_2)] \\
&= \frac{\chi\tau}{4\pi} \sum_{n=n_{\min}}^{n_{\max}} \frac{B_n}{n}, \quad (27)
\end{aligned}$$

where we used (15) and

$$\sum_n \left(\frac{B_n}{n}\right) = \left(\frac{2\pi}{\tau^2}\right) \int_0^\tau dt \int_0^t dt' g(t') dt'. \quad (28)$$

| mode number $p$ | $\omega_p/(2\pi)$ (MHz) |
|-----------------|-------------------------|
| 1               | 2.953                   |
| 2               | 2.966                   |
| 3               | 2.984                   |
| 4               | 3.006                   |
| 5               | 3.029                   |
| 6               | 3.049                   |
| 7               | 3.060                   |

TABLE I. Motional-mode frequencies  $\omega_p/(2\pi)$  (in MHz),  $p = 1, \dots, 7$ , used to construct the 7-ion AMFM test pulses.

| $p$ | $j = 1$  | $j = 2$  | $j = 3$  | $j = 4$  | $j = 5$  | $j = 6$  | $j = 7$  |
|-----|----------|----------|----------|----------|----------|----------|----------|
| 1   | 0.01033  | -0.03355 | 0.05478  | -0.06313 | 0.05478  | -0.03355 | 0.01033  |
| 2   | 0.02226  | -0.05627 | 0.05036  | 0.00000  | -0.05036 | 0.05627  | -0.02226 |
| 3   | -0.03494 | 0.05644  | 0.00760  | -0.05823 | 0.00760  | 0.05644  | -0.03494 |
| 4   | 0.04644  | -0.03074 | -0.05488 | 0.00000  | 0.05488  | 0.03074  | -0.04644 |
| 5   | 0.05503  | 0.00994  | -0.03678 | -0.05637 | -0.03678 | 0.00994  | 0.05503  |
| 6   | -0.05848 | -0.04491 | -0.02433 | 0.00000  | 0.02433  | 0.04491  | 0.05848  |
| 7   | 0.04143  | 0.04143  | 0.04143  | 0.04143  | 0.04143  | 0.04143  | 0.04143  |

TABLE II. Lamb-Dicke parameters  $\eta_p^j$ ,  $p, j = 1, \dots, 7$ , used to construct the 7-ion AMFM test pulses.

#### IV. GATE SIMULATOR

Given a Hamiltonian and enough computer power, one can always solve the time evolution of the computational states including phonon excitations to any desired accuracy. In this paper we focus on a 7-ion chain and expand the complete state  $|\psi(t)\rangle$  in the combined Hilbert space of computational states  $|a, b\rangle$ ,  $a, b \in \{0, 1\}$ , and phonon states  $|m_1 m_2 \dots m_7\rangle$ ,  $m_j = 0, 1, \dots, m_j^{\max}$ ,  $j = 1, \dots, 7$ , according to

$$|\psi(t)\rangle = \sum_{\substack{a,b \\ m_1, m_2, \dots, m_7}} A_{m_1 m_2 \dots m_7}^{(a,b)}(t) |a, b\rangle |m_1 m_2 \dots m_7\rangle, \quad (29)$$

where  $m_j^{\max} \geq 0$  is the maximal phonon occupation number included in the basis. We call  $\{m_1^{\max}, \dots, m_7^{\max}\}$  the phonon scheme. With (29), the time-dependent Schrödinger equation results in the amplitude equations

$$i\hbar \dot{A}_{n_1 n_2 \dots n_7}^{(a,b)}(t) = \sum_{\substack{a', b' \\ m_1, m_2, \dots, m_7}} \langle a, b | \langle n_1 \dots n_7 | \hat{H}(t) | m_1 \dots m_7 \rangle | a', b' \rangle A_{m_1 \dots m_7}^{(a', b')}(t), \quad (30)$$

where  $\hat{H}(t)$  may be any of the model Hamiltonians defined in Section II. The set of equations (30) are ordinary first-order differential equations that may be solved with any standard numerical differential equations solver. For simplicity and straightforward numerical error control, we chose an elementary fourth-order Runge-Kutta solver with constant step size [33]. With this simple integrator we are able to obtain a relative accuracy of the numerical solution of better than  $10^{-7}$ . Obviously, the gate simulator is not limited to 7 ions. It scales trivially to any number of ions. For the purposes of this paper we chose 7-ion chains as a compromise between a reasonably long ion chain and manageable computation times. The matrix elements that occur in (30) are computed in Section XVI (Appendix A).

Convergence in the phonon scheme is assessed by using the gate simulator to compute  $|\psi(\tau)\rangle$  for the Hamiltonian  $\hat{H}(t) = \hat{H}_S(t) = \hat{H}^{(-2,1)}(t)$ . In this case, we need to obtain full phase-space closure, because the control pulses are constructed on the basis of the same Hamiltonian that governs the time evolution. Only if enough phonon states are included in the basis used by the gate-simulator, will the phase space be closed and thus indicate that the phonon-space truncation according to the phonon scheme guarantees an accurate result.

## V. FIDELITY MEASURES

The ideal XX gate propagator is

$$\hat{U}_{\text{ideal}} = e^{i\chi\sigma_x^{(1)}\sigma_x^{(2)}}, \quad (31)$$

where  $\chi$  is the gate angle. For starting state  $|\psi_0\rangle$  this produces the ideal final state

$$|\psi_{\text{ideal}}\rangle = \hat{U}_{\text{ideal}}|\psi_0\rangle. \quad (32)$$

However, a given gate pulse  $g(t)$ , in general, produces a gate propagator of the form

$$\hat{U}_{\text{actual}} = e^{i[\chi\sigma_x^{(1)}\sigma_x^{(2)} + \lambda\hat{E}]}, \quad (33)$$

where  $\hat{E}$  is a hermitian error operator and  $\lambda$  is its strength. In this case, and for given initial state  $|\psi_0\rangle$ , we define the state fidelity according to

$$F_S = |\langle \psi_{\text{ideal}} | \psi_{\text{actual}} \rangle|^2 = \left| \langle \psi_0 | \hat{U}_{\text{ideal}}^\dagger \hat{U}_{\text{actual}} | \psi_0 \rangle \right|^2. \quad (34)$$

There are two types of error operators, i.e., those that commute with  $\sigma_x^{(1)}\sigma_x^{(2)}$  and those that do not. If only a single, commuting error operator  $\hat{E}$  is present, the state fidelity, up to second order in  $\lambda$ , is

$$F_S = \left| \langle \psi_0 | e^{-i\chi\sigma_x^{(1)}\sigma_x^{(2)}} e^{i\chi\sigma_x^{(1)}\sigma_x^{(2)} + \lambda\hat{E}} | \psi_0 \rangle \right|^2 = \left| \langle \psi_0 | e^{i\lambda\hat{E}} | \psi_0 \rangle \right|^2 = 1 - \lambda^2\sigma_{\hat{E}}^2, \quad (35)$$

where

$$\sigma_{\hat{E}}^2 = \langle \psi_0 | \hat{E}^2 | \psi_0 \rangle - \langle \psi_0 | \hat{E} | \psi_0 \rangle^2. \quad (36)$$

This means that the state infidelity

$$\bar{F}_S = 1 - F_S, \quad (37)$$

up to second order in  $\lambda$ , is

$$\bar{F}_S = \lambda^2\sigma_{\hat{E}}^2. \quad (38)$$

It is proportional to the square of the error strength.

In case the error operator  $\hat{E}$  does not commute with  $\sigma_x^{(1)}\sigma_x^{(2)}$ , we may use the Baker-Hausdorff-Campbell formula to obtain, up to second order in  $\lambda$ ,

$$\begin{aligned} F_S &= \left| \langle \psi_0 | \hat{U}_{\text{ideal}}^\dagger \hat{U}_{\text{actual}} | \psi_0 \rangle \right|^2 = \left| \langle \psi_0 | e^{-i\chi\sigma_x^{(1)}\sigma_x^{(2)}} e^{i\chi\sigma_x^{(1)}\sigma_x^{(2)} + i\lambda\hat{E}} | \psi_0 \rangle \right|^2 \\ &= \left| \langle \psi_0 | e^{i\lambda\hat{C} + i\lambda^2\hat{D} + \dots} | \psi_0 \rangle \right|^2 \\ &= \left| \langle \psi_0 | 1 + i\lambda(\hat{C} + \lambda\hat{D}) - \frac{1}{2}\lambda^2(\hat{C} + \lambda\hat{D})^2 + \dots | \psi_0 \rangle \right|^2 \\ &= 1 - \lambda^2\sigma_{\hat{C}}^2, \end{aligned} \quad (39)$$

where  $\hat{C}$  and  $\hat{D}$  are hermitian operators that can be expressed as linear combinations of nested multi-commutators of  $\sigma_x^{(1)}\sigma_x^{(2)}$  and  $\hat{E}$ . This implies that in this case, too, the infidelity  $\bar{F}_S$  is proportional to  $\lambda^2$ .

Most of the error operators  $\hat{E}$  that appear in the present context do not commute with  $\sigma_x^{(1)}\sigma_x^{(2)}$ . However, if  $\hat{E}$  can be written in the form  $\hat{E} = \hat{A}\hat{\Omega}$ , where  $\hat{A}$  is a hermitian error

operator in the computational space and  $\hat{\Omega}$  is a hermitian error operator in the phonon space, and if  $\hat{A}$  fulfills the anti-commutation relation

$$\left\{ \sigma_x^{(1)} \sigma_x^{(2)}, \hat{A} \right\} = \sigma_x^{(1)} \sigma_x^{(2)} \hat{A} + \hat{A} \sigma_x^{(1)} \sigma_x^{(2)} = 0, \quad (40)$$

we can compute  $\bar{F}_S$  explicitly, which also provides an explicit expression for the operator  $\hat{C}$  in (39). Examples of error operators  $\hat{A}$  that fulfill (40) are

$$\hat{A} \in \left\{ \sigma_y^{(1)}, \sigma_y^{(2)}, \sigma_z^{(1)}, \sigma_z^{(2)}, \sigma_x^{(1)} \sigma_y^{(2)}, \sigma_x^{(1)} \sigma_z^{(2)}, \sigma_x^{(2)} \sigma_y^{(1)}, \sigma_x^{(2)} \sigma_z^{(1)} \right\}. \quad (41)$$

Since they act in different spaces, we have

$$[\sigma_x^{(1)} \sigma_x^{(2)}, \hat{\Omega}] = 0, \quad [\hat{A}, \hat{\Omega}] = 0. \quad (42)$$

If (40) is fulfilled, we have

$$\begin{aligned} \hat{U}_{\text{actual}} &= e^{i\chi \sigma_x^{(1)} \sigma_x^{(2)} + i\lambda \hat{A} \hat{\Omega}} \\ &= \cos(\hat{\varphi}) + i \left( \frac{\sin(\hat{\varphi})}{\hat{\varphi}} \right) \left[ \chi \sigma_x^{(1)} \sigma_x^{(2)} + \lambda \hat{A} \hat{\Omega} \right], \end{aligned} \quad (43)$$

where

$$\hat{\varphi} = \sqrt{\chi^2 + \lambda^2 \hat{A}^2 \hat{\Omega}^2}. \quad (44)$$

Then, up to second order in  $\lambda$ , we have

$$\begin{aligned} F_S &= \left| 1 + i \left( \frac{\lambda}{\chi} \right) \cos(\chi) \sin(\chi) \langle \psi_0 | \hat{A} \hat{\Omega} | \psi_0 \rangle \right. \\ &\quad \left. + \left( \frac{\lambda}{\chi} \right) \sin^2(\chi) \langle \psi_0 | \sigma_x^{(1)} \sigma_x^{(2)} \hat{A} \hat{\Omega} | \psi_0 \rangle - \left( \frac{\lambda^2}{2\chi^2} \right) \sin^2(\chi) \hat{A}^2 \hat{\Omega}^2 \right|^2. \end{aligned} \quad (45)$$

Now, because of (40) and (42), we have

$$\begin{aligned} \langle \psi_0 | \sigma_x^{(1)} \sigma_x^{(2)} \hat{A} \hat{\Omega} | \psi_0 \rangle &= -\langle \psi_0 | \hat{A} \sigma_x^{(1)} \sigma_x^{(2)} \hat{\Omega} | \psi_0 \rangle = -\langle \psi_0 | \hat{\Omega} \sigma_x^{(1)} \sigma_x^{(2)} \hat{A} | \psi_0 \rangle^* \\ &= -\langle \psi_0 | \sigma_x^{(1)} \sigma_x^{(2)} \hat{A} \hat{\Omega} | \psi_0 \rangle^*. \end{aligned} \quad (46)$$

This means that  $\langle \psi_0 | \sigma_x^{(1)} \sigma_x^{(2)} \hat{A} \hat{\Omega} | \psi_0 \rangle$  is purely imaginary, and we may write

$$\langle \psi_0 | \sigma_x^{(1)} \sigma_x^{(2)} \hat{A} \hat{\Omega} | \psi_0 \rangle = i \Im \left\{ \langle \psi_0 | \sigma_x^{(1)} \sigma_x^{(2)} \hat{A} \hat{\Omega} | \psi_0 \rangle \right\}. \quad (47)$$

With this result, we now have, up to second order in  $\lambda$ :

$$\begin{aligned} F_S &= 1 - \left( \frac{\lambda^2}{\chi^2} \right) \sin^2(\chi) \langle \psi_0 | \hat{A}^2 \hat{\Omega}^2 | \psi_0 \rangle \\ &\quad + \left( \frac{\lambda^2}{\chi^2} \right) \sin^2(\chi) \left[ \cos(\chi) \langle \psi_0 | \hat{A} \hat{\Omega} | \psi_0 \rangle - i \sin(\chi) \langle \psi_0 | \sigma_x^{(1)} \sigma_x^{(2)} \hat{A} \hat{\Omega} | \psi_0 \rangle \right]^2 \\ &= 1 - \lambda^2 \sigma_C^2, \end{aligned} \quad (48)$$

where

$$\begin{aligned}\hat{C} &= \left(\frac{\sin(\chi)}{\chi}\right) \left[ \cos(\chi) \hat{A} \hat{\Omega} - i \sin(\chi) \sigma_x^{(1)} \sigma_x^{(2)} \hat{A} \hat{\Omega} \right] \\ &= \left(\frac{\sin(\chi)}{\chi}\right) e^{-i\chi \sigma_x^{(1)} \sigma_x^{(2)}} \hat{A} \hat{\Omega}.\end{aligned}\quad (49)$$

Notice that, because of (42), and since  $\hat{A}$  is assumed to fulfill (40),  $i\sigma_x^{(1)}\sigma_x^{(2)}\hat{A}\hat{\Omega}$  is a hermitian operator. So,  $\hat{C}$  is hermitian, as it should be, and  $\hat{C}^2 = \hat{C}^\dagger \hat{C}$ . With this result, we have explicitly

$$\bar{F}_S = \left(\frac{\lambda \sin(\chi)}{\chi}\right)^2 \left\{ \langle \psi_0 | \hat{A}^2 \hat{\Omega}^2 | \psi_0 \rangle - \langle \psi_0 | e^{-i\chi \hat{\sigma}_x^{(1)} \hat{\sigma}_x^{(2)}} \hat{A} \hat{\Omega} | \psi_0 \rangle^2 \right\}.\quad (50)$$

The explicit form (48) of  $F_S$  confirms the general result (39) in cases where the condition (40) is met. Many of the most important error operators occurring in this paper satisfy (40) and thus (50) is applicable.

In the case of a two-qubit gate, the error operator takes the form  $\hat{E} = \sum_{j=1,2} \hat{A}^{(j)} \hat{\Omega}^{(j)}$ . In this case (48), (49), and (50) may immediately be generalized using the substitution

$$\hat{A} \hat{\Omega} \rightarrow \sum_{j=1,2} \hat{A}^{(j)} \hat{\Omega}^{(j)}.\quad (51)$$

The output of the gate simulator code is the complete state  $|\psi_{\text{out}}^M(\tau)\rangle$ , which includes computational states and phonon states. This way, we possess the complete state information, which can be used to compute the state fidelity defined in (34) with  $|\psi_{\text{actual}}\rangle = |\psi_{\text{out}}^M(\tau)\rangle$ . In Section VI we use the state fidelity  $F_S$  to assess the quality of the various model Hamiltonians  $\hat{H}_M^{(N_c, N_s)}$ .

The state fidelity  $F_S$ , as defined in (34), depends on the initial state  $|\psi_0\rangle$ . A more global measure of the fidelity of the quantum process that implements the two-qubit XX gate is the process fidelity

$$F_P = \frac{1}{16} \text{Tr} \left[ \mathcal{E}_{\text{exact}}^\dagger \mathcal{E}_{\text{actual}} \right],\quad (52)$$

where  $\mathcal{E}_{\text{exact}}$  is the exact XX gate process and  $\mathcal{E}_{\text{actual}}$  is the actual two-qubit XX-gate process as computed with the gate simulator as described in Section IV.

A related fidelity measure, also used in Section VI, is the average gate fidelity  $F_G$ . In our case, following [34],  $F_G$  is defined according to

$$F_G = \frac{1}{80} \sum_{j=1}^{16} \text{Tr} \left[ \hat{U}_{\text{exact}} \hat{U}_j^\dagger \hat{U}_{\text{exact}}^\dagger \mathcal{E}(\hat{U}_j) \right],\quad (53)$$

where  $\hat{U}_j$ ,  $j = 1, \dots, 16$ , is an operator basis in the computational space as defined in [34].

In addition to the state infidelity  $\bar{F}_S = 1 - F_S$ , defined in (37), we define the infidelities

$$\begin{aligned}\bar{F}_G &= 1 - F_G, \\ \bar{F}_P &= 1 - F_P.\end{aligned}\tag{54}$$

For characterizing the quality of the various Hamiltonians investigated in this paper, it is useful to define the error in the gate angle

$$\Delta\chi = \chi - \frac{\pi}{4},\tag{55}$$

where  $\chi$  is the actual gate angle computed by running the XX gate simulator (see Sections IV and VI). A positive  $\Delta\chi$  corresponds to an over-rotated gate angle  $\chi$ , while a negative  $\Delta\chi$  corresponds to an under-rotated gate angle  $\chi$ . The error operator associated with  $\Delta\chi$  is  $\hat{E}_\chi = \Delta\chi \hat{\sigma}_x^{(1)} \hat{\sigma}_x^{(2)}$ . Then, according to (35), for  $|\psi_0\rangle = |00\rangle|\text{ph}\rangle$ , for instance, where  $|00\rangle$  is the computational state and  $|\text{ph}\rangle$  is any normalized phonon state, the state infidelity caused by  $\hat{E}_\chi$  is

$$\bar{F}_S^{(\chi)} = (\Delta\chi)^2.\tag{56}$$

## VI. NUMERICAL RESULTS

As described in Section III, we computed AMFM pulse functions  $g(t)$  for gate times ranging from  $\tau = 100\mu\text{s}$  to  $\tau = 600\mu\text{s}$  in steps of  $100\mu\text{s}$ , and used these pulse functions in the XX gate simulator (see Section IV). As described in Section IV, using the full Hamiltonian  $\hat{H}_{MS}$  defined in (5), we computed the full state function  $|\psi(\tau)\rangle$  that includes both the computational space and the phonon space. From  $|\psi(\tau)\rangle$ , as described in Section V, we then computed the infidelities  $\bar{F}_S$ ,  $\bar{F}_G$ ,  $\bar{F}_P$ , and the error  $\Delta\chi$  in the gate angle  $\chi$ . The results are shown in Table III.

Accepting  $\hat{H}_{MS}$  as a good approximation of  $\hat{H}_R$ , the most important result we obtain from Table III is that a gate infidelity  $< 10^{-4}$  cannot be achieved if the control pulses  $g(t)$  are constructed on the basis of the standard Hamiltonian  $\hat{H}_S$ . Nevertheless, while not quite meeting the goal of  $\lesssim 10^{-4}$ , the infidelities obtained are very close to this goal. We also see

| $\tau$               | 100      | 200      | 300      | 400      | 500      | 600      |
|----------------------|----------|----------|----------|----------|----------|----------|
| phonon scheme        | 22551111 | 45221111 | 26211111 | 26211111 | 26211111 | 26211111 |
| $\bar{F}_S$          | 3.1      | 2.6      | 4.0      | 1.9      | 2.5      | 1.7      |
| $\bar{F}_G$          | 2.4      | 2.1      | 3.1      | 1.5      | 2.0      | 1.3      |
| $\bar{F}_P$          | 3.0      | 2.6      | 3.8      | 1.8      | 2.5      | 1.6      |
| $\Delta\chi$         | -0.012   | -0.011   | -0.011   | -0.011   | -0.011   | -0.011   |
| $\bar{F}_S^c$        | 1.6      | 1.5      | 2.9      | 0.78     | 1.4      | 0.61     |
| $\bar{F}_G^c$        | 1.3      | 1.2      | 2.2      | 0.56     | 1.1      | 0.47     |
| $\bar{F}_P^c$        | 1.6      | 1.5      | 2.7      | 0.70     | 1.4      | 0.58     |
| $\bar{F}_S^{\Phi,c}$ | 0.88     | 0.14     | 0.62     | 0.41     | 0.34     | 0.45     |
| $\bar{F}_G^{\Phi,c}$ | 0.67     | 0.10     | 0.36     | 0.28     | 0.26     | 0.34     |
| $\bar{F}_P^{\Phi,c}$ | 0.84     | 0.12     | 0.45     | 0.34     | 0.32     | 0.42     |

TABLE III. Phonon schemes and infidelities for XX gate between ion pair (2,5) as a function of gate time  $\tau$  in  $\mu\text{s}$ . All infidelities are in units of  $10^{-4}$ . Thus, table entries  $< 1$  correspond to infidelities below the  $10^{-4}$  infidelity target.  $\bar{F}_S$ ,  $\bar{F}_G$ , and  $\bar{F}_P$  are the state-, average gate-, and process infidelities obtained with control pulses constructed on the basis of  $\hat{H}_C(t) = \hat{H}_S(t)$ .  $\Delta\chi$  is negative, which indicates that  $\hat{H}_C(t) = \hat{H}_S(t)$  under-rotates the gate angle  $\chi$ .  $\bar{F}_S^c$ ,  $\bar{F}_G^c$ , and  $\bar{F}_P^c$  are obtained with the calibrated pulse  $cg(t)$ , where  $c$  is the calibration factor [see (58)].  $\bar{F}_S^{\Phi,c}$ ,  $\bar{F}_G^{\Phi,c}$ , and  $\bar{F}_P^{\Phi,c}$  are obtained with a control pulse that is constructed with the  $\Phi$ -condition (122) added and subsequently calibrated. The table shows that in this case all infidelities are suppressed below  $10^{-4}$ .

that the three different infidelity measures, i.e.,  $\bar{F}_S$ ,  $\bar{F}_G$ , and  $\bar{F}_P$  yield similar results and any one of them may be used as a proxy for assessing the infidelity of the two-qubit XX gate.

Next, we fix the control pulse  $g(t)$  (we use the  $300\ \mu\text{s}$  pulse from Table III) and determine the quality of the various approximations  $\hat{H}_M^{(N_c, N_s)}$  to the full Hamiltonian  $\hat{H}_{MS}$  by computing  $\bar{F}_P$  for some of the Hamiltonians  $\hat{H}_M^{(N_c, N_s)}$ . The result is shown in Table IV. We see that, expectedly,  $\bar{F}_P \ll 10^{-4}$  for  $\hat{H}_M^{(-2,1)} = \hat{H}_S$ , since in this case the pulse is generated on the basis of  $\hat{H}_S$  and the gate simulator is controlled by  $\hat{H}_S$  as well. So, ideally, we should obtain perfect fidelity. The difference from zero in Table IV in this case is not due to the accuracy of the numerical integrator, which, as stated in Section IV is of the order of  $10^{-7}$ , but is due



to the phonon scheme. Including more phonon states in our basis increases the accuracy of our simulations and drives the infidelity in the case of  $\hat{H}_M^{(N_c=-2, N_s=1)} = \hat{H}_S$  closer to zero. The table entry for  $(N_c = -2, N_s = 1)$  also provides us with an estimate of the accuracy of the infidelity entries in Tables III and IV. As indicated by the  $(N_c = -2, N_s = 1)$  entry in Table IV, the phonon schemes we chose guarantee an accuracy of the computed infidelities of approximately  $3 \times 10^{-5}$ .

Looking at the infidelity results in Table IV for the Hamiltonians expanded to zeroth and second orders in the cos-term in (5), we see that neglecting the zeroth-order term in (5) (the carrier term) is not justified. But we also see that, apparently, expansion to second order of the cos-term of (5) is not necessary. This is shown analytically in more detail in Sections VIII B and VIII C.

Turning now to the expansions of the sin-term of (5), Table IV shows that truncating this expansion at the first order of the sin function, i.e., linearizing the sin-term in the Lamb-Dicke parameters, is not accurate enough. As a consequence, the expansion of the sin term in (5) has to be carried to the third order in the Lamb-Dicke parameters, but expansion to the 5th order is not necessary.

As an overall result of the performance tests for different  $(N_c, N_s)$  model Hamiltonians we obtain that  $\hat{H}_M^{(0,3)}$  is a good enough approximation of  $\hat{H}_{MS}$  on the  $\lesssim 10^{-4}$  fidelity level. Conversely, we also obtain the important result that pulse construction on the basis of the standard Hamiltonian  $\hat{H}_S = \hat{H}_M^{(-2,1)}$  does not yield infidelities  $< 10^{-4}$ . Thus, to improve control-pulse construction, at a minimum, we have to include the carrier term [zeroth-order cos term in (5)] and the third-order sin term in (5). In Sections VIII B and VIII C, we explore the effects of these two additional Hamiltonian terms. We also show analytically that inclusion of the second- and fourth-order terms of the Hamiltonian (5) are not needed.

## VII. CALIBRATION

Table III shows that  $\Delta\chi$  is quite large and may make a significant contribution to the infidelity. However, by slightly adjusting the amplitude of the control pulse  $g(t)$ , we are able to completely eliminate  $\Delta\chi$  and thus eliminate any contribution to the infidelity that otherwise would be due to  $\Delta\chi$ . Adjusting  $g(t)$  to result in  $\Delta\chi = 0$  is called calibration. This

|                | $N_s = 1$ | $N_s = 3$ | $N_s = 5$ | $N_s = \infty$ |
|----------------|-----------|-----------|-----------|----------------|
| $N_c = -2$     | 0.31      | 1.6       | 1.6       | 1.6            |
| $N_c = 0$      | 2.5       | 3.8       | 3.8       | –              |
| $N_c = 2$      | 2.5       | 3.8       | 3.8       | –              |
| $N_c = \infty$ | –         | –         | –         | 3.8            |

TABLE IV. Process infidelities  $\bar{F}_P$  in units of  $10^{-4}$  for phonon scheme 2621111 and ion pair (2,5) produced by model Hamiltonians  $H_M^{(N_c, N_s)}$ . A dash in the table means that the corresponding quantity was not computed.

procedure, extensively used in the laboratory, is an attractive way of reducing the infidelity, since the phase-space closure conditions (14), linear in the amplitude of the control pulse  $g(t)$ , are invariant under a change in the control-pulse amplitude. So, despite calibration of the pulse, phase-space closure is always guaranteed exactly, independent of the pulse amplitude.

The error operator for  $\Delta\chi$  is  $\hat{E} = \Delta\chi \hat{\sigma}_x^{(1)} \hat{\sigma}_x^{(2)}$ , which trivially commutes with  $\hat{\sigma}_x^{(1)} \hat{\sigma}_x^{(2)}$ . Therefore, for all entries in Table III, the contribution of  $\Delta\chi$  to the infidelity may be estimated according to (35) and (36) as

$$\bar{F}_S^{(\Delta\chi)} = (\Delta\chi)^2 [1 - \langle \psi_0 | \sigma_x^{(1)} \sigma_x^{(2)} | \psi_0 \rangle^2]. \quad (57)$$

Based on this result, and for all pulse lengths listed in Table III, we have  $\bar{F}_S^{(\Delta\chi)} \sim 1.2 \times 10^{-4}$ , which makes a significant contribution to the infidelities listed in Table III. However, as mentioned above, this infidelity may be eliminated by calibrating the control pulse. Denoting by  $\chi_{\text{target}}$  the desired degree of entanglement and by  $\chi_g = \chi_{\text{target}} + \Delta\chi$  the degree of entanglement actually obtained with the control pulse  $g(t)$ , the calibration factor  $c$ , i.e., the (real) factor by which the amplitude of  $g(t)$  has to be multiplied to eliminate  $\Delta\chi$  is obtained explicitly, with (15), as

$$c = (\chi_{\text{target}}/\chi_g)^{1/2} = \left( \frac{\chi_{\text{target}}}{\chi_{\text{target}} + \Delta\chi} \right)^{1/2}. \quad (58)$$

The entries for  $F_S^c$ ,  $F_G^c$ , and  $F_P^c$  in Table III represent the results for the respective infidelities computed with the same control pulses used for the corresponding entries  $F_S$ ,  $F_G$ , and  $F_P$ , but multiplied (calibrated) with the calibration factor  $c$ , computed according to (58) with

the corresponding  $\Delta\chi$  values from Table III and  $\chi_{\text{target}} = \pi/4$ . As expected, the result is a significant reduction of the infidelity. Since the starting state  $|\psi_0\rangle$  for the results in Table III is  $|\psi_0\rangle = |00\rangle|0\rangle_{\text{ph}}$ , we expect a reduction by  $\Delta\chi^2$ . This agrees well with the results in Table III. Since they can no longer be due to  $\Delta\chi$ , the rest of the infidelities in Table III have to come from other sources that are not proportional to  $(\Delta\chi)^2$ . To look for these sources, we now compute the XX-gate propagator via a Magnus expansion as outlined in the following section.

### VIII. MAGNUS EXPANSION

Given the time-dependent Schrödinger equation

$$i\hbar\frac{\partial}{\partial t}|\psi(t)\rangle = \hat{H}(t)|\psi(t)\rangle, \quad (59)$$

the time evolution operator  $\hat{U}(\tau)$  of (59) over the time interval  $\tau$  may be constructed systematically and analytically, using a Magnus expansion [35], i.e., up to 3rd order in the Hamiltonian:

$$\hat{U}(\tau) = \exp\left[i\hat{W}_1(\tau) + i\hat{W}_2(\tau) + i\hat{W}_3(\tau) + \dots\right], \quad (60)$$

where

$$\begin{aligned} \hat{W}_1(\tau) &= \frac{1}{i} \int_0^\tau \left(-\frac{i}{\hbar}\right) \hat{H}(t_1) dt_1, \\ \hat{W}_2(\tau) &= \frac{1}{2i} \int_0^\tau dt_1 \int_0^{t_1} dt_2 \left[ \left(-\frac{i}{\hbar}\right) \hat{H}(t_1), \left(-\frac{i}{\hbar}\right) \hat{H}(t_2) \right], \\ \hat{W}_3(\tau) &= \frac{1}{6i} \int_0^\tau dt_1 \int_0^{t_1} dt_2 \int_0^{t_2} dt_3 \\ &\quad \left\{ \left[ \left(-\frac{i}{\hbar}\right) \hat{H}(t_1), \left[ \left(-\frac{i}{\hbar}\right) \hat{H}(t_2), \left(-\frac{i}{\hbar}\right) \hat{H}(t_3) \right] \right] \right. \\ &\quad \left. + \left[ \left(-\frac{i}{\hbar}\right) \hat{H}(t_3), \left[ \left(-\frac{i}{\hbar}\right) \hat{H}(t_2), \left(-\frac{i}{\hbar}\right) \hat{H}(t_1) \right] \right] \right\} \end{aligned} \quad (61)$$

are hermitian operators.

In this section, we aim at a consistent Magnus expansion up to 4th order in the Lamb-Dicke parameters  $\eta_p^j$ . Therefore, expanding the cosine-term in (5) up to fourth order in  $\hat{V}_j$  and the sine-term in (5) up to third order in  $\hat{V}_j$  we use the Hamiltonian

$$\hat{H}(t) = \hbar g(t) \sum_{\alpha=0}^4 \hat{h}_\alpha(t) \quad (62)$$

in the Magnus expansion (61), where

$$\begin{aligned}
\hat{h}_0(t) &= \sum_j \sigma_y^{(j)}, \\
\hat{h}_1(t) &= \sum_j \hat{V}_j(t) \hat{\sigma}_x^{(j)}, \\
\hat{h}_2(t) &= -\frac{1}{2} \sum_j \hat{V}_j^2(t) \hat{\sigma}_y^{(j)}, \\
\hat{h}_3(t) &= -\frac{1}{6} \sum_j \hat{V}_j^3(t) \hat{\sigma}_x^{(j)}, \\
\hat{h}_4(t) &= \frac{1}{24} \sum_j \hat{V}_j^4(t) \hat{\sigma}_y^{(j)}.
\end{aligned} \tag{63}$$

Notice that  $\hat{h}_0(t)$  is actually time independent, but we formally keep the time argument for notational convenience. Based on the results listed in Table IV, we know that the zeroth order of  $\cos[\hat{V}_j(t)]$  contributes substantially to the infidelity, while the 2nd and higher orders of  $\cos[\hat{V}_j(t)]$  do not. We also know that the first and third orders of  $\sin[\hat{V}_j(t)]$  contribute substantially, while the 5th and higher orders do not. Thus, the Hamiltonian (62) covers all these important cases. According to Table IV, it may not be necessary to include the second- and fourth-order expansion terms of the cosine function in (5). However, for a consistent expansion up to fourth order in the Lamb-Dicke parameters, and also to show that these terms are negligible, we include them in our expansion (62) of (5).

We start in Section VIII A by computing  $\hat{W}_1(\tau)$  on the basis of (62), followed in Sections VIII B and VIII C by constructing  $\hat{W}_2(\tau)$  and  $\hat{W}_3(\tau)$ , respectively. We will find that many of the resulting error terms are negligible. But we will also identify the most significant terms that make significant contributions to the infidelity.

With the operators defined in (63), we define the hermitian operators

$$\hat{T}_\alpha = - \int_0^\tau \hat{h}_\alpha(t) g(t) dt, \quad \alpha = 0, 1, 2, 3, 4, \tag{64}$$

$$\hat{T}_{\alpha\beta} = -\frac{1}{2i} \int_0^\tau dt_1 \int_0^{t_1} dt_2 g(t_1)g(t_2) [\hat{h}_\alpha(t_1), \hat{h}_\beta(t_2)], \quad \alpha, \beta = 0, 1, 2, 3, 4, \tag{65}$$

and

$$\begin{aligned}
\hat{T}_{\alpha\beta\gamma} &= \left(\frac{1}{6}\right) \int_0^\tau dt_1 \int_0^{t_1} dt_2 \int_0^{t_2} dt_3 g(t_1)g(t_2)g(t_3) \\
&\quad \left\{ [\hat{h}_\alpha(t_1), [\hat{h}_\beta(t_2)], \hat{h}_\gamma(t_3)] + [\hat{h}_\alpha(t_3), [\hat{h}_\beta(t_2)], \hat{h}_\gamma(t_1)] \right\}, \quad \alpha, \beta, \gamma = 0, 1, 2, 3, 4.
\end{aligned} \tag{66}$$

In the following sections, these operators are used (i) to compute  $\hat{W}_1$ ,  $\hat{W}_2$ , and  $\hat{W}_3$  and (ii) to compute infidelity contributions to the gate evolution operator  $\hat{U}(\tau)$  defined in (60).

### A. First Order

With the definition in (64) we have

$$\hat{W}_1(\tau) = \sum_{\alpha=0}^4 \hat{T}_\alpha(\tau). \quad (67)$$

We use (13) together with

$$\int_0^\tau g(t) e^{i\omega_p t} dt = 0 \quad \Rightarrow \quad \int_0^\tau g(t) \hat{V}_j(t) dt = 0, \quad (68)$$

to arrive at

$$\hat{T}_0(\tau) = 0, \quad (69)$$

$$\hat{T}_1(\tau) = 0, \quad (70)$$

$$\hat{T}_2(\tau) = \left(\frac{1}{2}\right) \sum_{pqj} \eta_p^j \eta_q^j \hat{\sigma}_y^{(j)} [Q(\omega_p + \omega_q) \hat{a}_p^\dagger \hat{a}_q^\dagger + h.c.] + \sum_{pqj, p \neq q} \eta_p^j \eta_q^j \hat{\sigma}_y^{(j)} Q(\omega_p - \omega_q) \hat{a}_p^\dagger \hat{a}_q, \quad (71)$$

$$\begin{aligned} \hat{T}_3(\tau) &= \frac{1}{6} \sum_{j=1,2} \hat{\sigma}_x^{(j)} \int_0^\tau g(t) \hat{V}_j^3(t) dt \\ &= \frac{1}{6} \sum_{p,q,r,j} \eta_p^j \eta_q^j \eta_r^j \hat{\sigma}_x^{(j)} \left\{ Q(\omega_p + \omega_q + \omega_r) \hat{a}_p^\dagger \hat{a}_q^\dagger \hat{a}_r^\dagger + Q(\omega_p + \omega_q - \omega_r) \hat{a}_p^\dagger \hat{a}_q^\dagger \hat{a}_r \right. \\ &\quad \left. + Q(\omega_p - \omega_q + \omega_r) \hat{a}_p^\dagger \hat{a}_q \hat{a}_r^\dagger + Q(-\omega_p + \omega_q + \omega_r) \hat{a}_p \hat{a}_q^\dagger \hat{a}_r^\dagger + h.c. \right\}, \quad (72) \end{aligned}$$

and

$$\begin{aligned} \hat{T}_4(\tau) &= \left(-\frac{1}{24}\right) \sum_j \hat{\sigma}_y^{(j)} \int_0^\tau g(t) \hat{V}_j^4(t) dt \\ &= \left(-\frac{1}{24}\right) \sum_j \hat{\sigma}_y^{(j)} \int_0^\tau g(t) \sum_{pqrs} \eta_p^j \eta_q^j \eta_r^j \eta_s^j \\ &\quad \left\{ \hat{a}_p^\dagger \hat{a}_p^\dagger \hat{a}_r^\dagger \hat{a}_s^\dagger e^{i(\omega_p + \omega_q + \omega_r + \omega_s)t} + \hat{a}_p^\dagger \hat{a}_p^\dagger \hat{a}_r^\dagger \hat{a}_s e^{i(\omega_p + \omega_q + \omega_r - \omega_s)t} \dots \right\}, \quad (73) \end{aligned}$$

where we used  $Q(w)$  defined in (22), in particular, with (13),  $Q(0) = 0$ .

While  $\hat{T}_0(\tau)$  and  $\hat{T}_1(\tau)$  vanish,  $\hat{T}_2(\tau)$ ,  $\hat{T}_3(\tau)$ , and  $\hat{T}_4(\tau)$  need to be investigated further since they may produce undesirable contributions to the infidelity of the XX gate.

According to (71), the size of  $\hat{T}_2(\tau)$  is controlled by

$$\gamma_2 = \max_{pqj, \sigma=\pm 1} |\eta_p^j \eta_q^j Q(\omega_p + \sigma \omega_q)|. \quad (74)$$

Numerically, for the 300  $\mu\text{s}$  test pulse, we obtain

$$\gamma_2 = 3.5 \times 10^{-6}. \quad (75)$$

Since  $\gamma_2$  is significantly smaller than  $10^{-4}$ ,  $\hat{T}_2(\tau)$  may be neglected.

According to (72), the size of  $\hat{T}_3(\tau)$  is controlled by

$$\gamma_3^{(+)} = \left(\frac{1}{6}\right) \max_{pqrj} |\eta_p^j \eta_q^j \eta_r^j Q(\omega_p + \omega_q + \omega_r)| \quad (76)$$

and

$$\begin{aligned} \gamma_3^{(-)} &= \left(\frac{1}{6}\right) \max_{pqrj} |\eta_p^j \eta_q^j \eta_r^j Q(\omega_p + \omega_q - \omega_r)| = \left(\frac{1}{6}\right) \max_{pqrj} |\eta_p^j \eta_q^j \eta_r^j Q(\omega_p - \omega_q + \omega_r)| \\ &= \left(\frac{1}{6}\right) \max_{pqrj} |\eta_p^j \eta_q^j \eta_r^j Q(-\omega_p + \omega_q + \omega_r)|. \end{aligned} \quad (77)$$

For the 300  $\mu\text{s}$  test pulse we obtain

$$\begin{aligned} \gamma_3^{(+)} &= 5.8 \times 10^{-8}, \\ \gamma_3^{(-)} &= 3.1 \times 10^{-4}. \end{aligned} \quad (78)$$

Since  $\hat{\sigma}_x^{(j)}$  commutes with  $\hat{\sigma}_x^{(1)} \hat{\sigma}_x^{(2)}$ , we may use (35) to estimate the infidelity  $\bar{F}_S^{(T_3)}$  caused by  $\hat{T}_3(\tau)$ . Since, according to (78), both  $\gamma_3^{(+)}$  and  $\gamma_3^{(-)}$  are smaller than  $10^{-3}$ , and since  $\bar{F}_S^{(T_3)}$ , according to (35), involves the square of  $\hat{T}_3(\tau)$ , the infidelity caused by  $\hat{T}_3(\tau)$  is negligible on the level of  $10^{-4}$ .

According to (73), the size of  $\hat{T}_4(\tau)$  is controlled by

$$\gamma_4 = \max_{\substack{j,pqrs \\ \sigma_p \sigma_q \sigma_r \sigma_s = \pm 1}} |\eta_p^j \eta_q^j \eta_r^j \eta_s^j Q(\sigma_p \omega_p + \sigma_q \omega_q + \sigma_r \omega_r + \sigma_s \omega_s)|. \quad (79)$$

For the 300  $\mu\text{s}$  test pulse we obtain

$$\gamma_4 = 1.1 \times 10^{-7}. \quad (80)$$

Therefore,  $\hat{T}_4(\tau)$  can be neglected.

As a result of this section we obtain that, on the  $10^{-4}$  level, the first-order terms in the Magnus expansion do not contribute to the infidelity. We need to be careful however to recall that this is only true if the pulse function  $g(t)$  satisfies the condition (13). Thus, (13) is an important condition that needs to be required for high-fidelity XX gates.

## B. Second Order

We now turn to the evaluation of the second-order terms (65) in the Magnus expansion, i.e., we compute  $\hat{W}_2(\tau)$  analytically for  $\hat{H}(t)$  defined in (62) up to fourth order in the Lamb-Dicke parameters  $\eta$ . With the definitions (65) of the operators  $\hat{T}_{\alpha\beta}(\tau)$ , the definition (15) of the degree of entanglement, making use of (13), and the functions defined in (16) – (28), we obtain

$$\hat{W}_2(\tau) = \sum_{\alpha,\beta=0}^4 \hat{T}_{\alpha\beta}(\tau), \quad (81)$$

where the operators  $\hat{T}_{\alpha\beta}$ , listed only up to fourth order in  $\eta$ , are

$$\hat{T}_{00} = 0, \quad (82)$$

$$\begin{aligned} \hat{T}_{01} &= - \sum_{j=1,2} \hat{\sigma}_z^{(j)} \int_0^\tau g(t) G(t) \hat{V}_j(t) dt \\ &= - \sum_{jp} \eta_p^j \hat{\sigma}_z^{(j)} [f(\omega_p) \hat{a}_p^\dagger + f^*(\omega_p) \hat{a}_p], \end{aligned} \quad (83)$$

$$\hat{T}_{02} = 0, \quad (84)$$

$$\begin{aligned} \hat{T}_{03} &= \left(\frac{1}{6}\right) \sum_{j=1,2} \hat{\sigma}_z^{(j)} \int_0^\tau g(t) G(t) \hat{V}_j^3(t) dt \\ &= \left(\frac{1}{6}\right) \sum_{pqrj} \hat{\sigma}_z^{(j)} \eta_p^j \eta_q^j \eta_r^j \left\{ f(\omega_p + \omega_q + \omega_r) \hat{a}_p^\dagger \hat{a}_q^\dagger \hat{a}_r^\dagger + f(\omega_p + \omega_q - \omega_r) \hat{a}_p^\dagger \hat{a}_q^\dagger \hat{a}_r \right. \\ &\quad \left. + f(\omega_p - \omega_q + \omega_r) \hat{a}_p^\dagger \hat{a}_q \hat{a}_r^\dagger + f(-\omega_p + \omega_q + \omega_r) \hat{a}_p \hat{a}_q^\dagger \hat{a}_r^\dagger + h.c. \right\}, \end{aligned} \quad (85)$$

$$\hat{T}_{04} = 0, \quad (86)$$

$$\hat{T}_{10} = \hat{T}_{01}, \quad (87)$$

$$\hat{T}_{11} = \tilde{\chi} + \chi \hat{\sigma}_x^{(1)} \hat{\sigma}_x^{(2)}, \quad (88)$$

$$\begin{aligned} \hat{T}_{12} &= \left(\frac{1}{4}\right) \sum_j \hat{\sigma}_z^{(j)} \int_0^\tau dt_1 \int_0^{t_1} dt_2 g(t_1) g(t_2) \left\{ \hat{V}_j(t_1), \hat{V}_j^2(t_2) \right\} \\ &\quad - \sum_{pq, j \neq k} \eta_p^j \eta_p^k \eta_q^k \hat{\sigma}_x^{(j)} \hat{\sigma}_y^{(k)} [S_p(\omega_q) \hat{a}_q^\dagger + S_p^*(\omega_q) \hat{a}_q], \end{aligned} \quad (89)$$

$$\begin{aligned}
\hat{T}_{13} &= \left(-\frac{1}{2}\right) \sum_{jkp} \hat{\sigma}_x^{(j)} \hat{\sigma}_x^{(k)} \eta_p^j \eta_p^k \int_0^\tau dt_1 \int_0^{t_1} dt_2 g(t_1) g(t_2) \sin[\omega_p(t_1 - t_2)] \hat{V}_j^2(t_1) \\
&= \left(-\frac{1}{2}\right) \sum_{jkpqr} \hat{\sigma}_x^{(j)} \hat{\sigma}_x^{(k)} \eta_p^j \eta_p^k \eta_q^j \eta_r^j [S_p(\omega_q + \omega_r) \hat{a}_q^\dagger \hat{a}_r^\dagger \\
&\quad + S_p(\omega_q - \omega_r) \hat{a}_q^\dagger \hat{a}_r + S_p^*(\omega_q - \omega_r) \hat{a}_q \hat{a}_r^\dagger + S_p^*(\omega_q + \omega_r) \hat{a}_q \hat{a}_r], \tag{90}
\end{aligned}$$

$$\hat{T}_{20} = 0, \tag{91}$$

$$\hat{T}_{21} = \hat{T}_{12}, \tag{92}$$

$$\hat{T}_{22} = \left(\frac{1}{2}\right) \sum_{jkp} \eta_p^j \eta_p^k \hat{\sigma}_y^{(j)} \hat{\sigma}_y^{(k)} \int_0^\tau dt_1 \int_0^{t_1} dt_2 g(t_1) g(t_2) \sin[\omega_p(t_1 - t_2)] \left\{ \hat{V}_j(t_1), \hat{V}_k(t_2) \right\}, \tag{93}$$

$$\hat{T}_{30} = \hat{T}_{03}, \tag{94}$$

$$\hat{T}_{31} = T_{13}, \tag{95}$$

and

$$\hat{T}_{40} = 0. \tag{96}$$

The above explicit, analytical results are computed making explicit use of (13).

Since  $\tilde{\chi}$  in (93) is only a c-number, which causes only a phase,  $\hat{T}_{11}$  generates the desired XX gate. All the other operators  $\hat{T}_{\alpha\beta}$  in (82) – (96), if not identically zero, are unwanted error operators that generate infidelities. Because of the symmetries and the operators that are identically zero, we have to investigate the sizes of only five remaining, non-zero error operators, i.e.,  $\hat{T}_{01}$ ,  $\hat{T}_{03}$ ,  $\hat{T}_{12}$ ,  $\hat{T}_{13}$ , and  $\hat{T}_{22}$ .

The size of  $\hat{T}_{01}$  is controlled by

$$\gamma_{01} = \max_{pj} |\eta_p^j f(\omega_p)|. \tag{97}$$

For the 300  $\mu\text{s}$  test pulse we obtain

$$\gamma_{01} = 1.8 \times 10^{-6}. \tag{98}$$

Thus, on the  $10^{-4}$  level,  $\hat{T}_{01}$  can safely be neglected.

Next, we turn to the evaluation of  $\hat{T}_{03}$ , which proceeds in analogy to the evaluation of  $\hat{T}_3(\tau)$  in Section VIII A. The size of  $\hat{T}_{03}$  is controlled by

$$\gamma_{03}^{(+)} = \left(\frac{1}{6}\right) \max_{pqrj} |\eta_p^j \eta_q^j \eta_r^j f(\omega_p + \omega_q + \omega_r)| \tag{99}$$



and

$$\begin{aligned}\gamma_{03}^{(-)} &= \left(\frac{1}{6}\right) \max_{pqrj} |\eta_p^j \eta_q^j \eta_r^j f(\omega_p + \omega_q - \omega_r)| = \left(\frac{1}{6}\right) \max_{pqrj} |\eta_p^j \eta_q^j \eta_r^j f(\omega_p - \omega_q + \omega_r)| \\ &= \left(\frac{1}{6}\right) \max_{pqrj} |\eta_p^j \eta_q^j \eta_r^j f(-\omega_p + \omega_q + \omega_r)|.\end{aligned}\quad (100)$$

For the 300  $\mu\text{s}$  test pulse we obtain

$$\begin{aligned}\gamma_{03}^{(+)} &= 7.4 \times 10^{-10}, \\ \gamma_{03}^{(-)} &= 9.3 \times 10^{-10}.\end{aligned}\quad (101)$$

Thus,  $\hat{T}_{03}$  is negligible.

According to (89), the operator  $\hat{T}_{12}$  consists of two parts, an anti-commutator part and a part that originated from a commutator. The size of the anti-commutator part of  $\hat{T}_{12}$  is controlled by

$$\gamma_{12}^{(a)} = \max_{\substack{j,pqr \\ \sigma_p \sigma_q \sigma_r = \pm 1}} |\eta_p^j \eta_q^j \eta_r^j Z(\sigma_p \omega_p, \sigma_q \omega_q + \sigma_r \omega_r)|.\quad (102)$$

The commutator part is controlled by

$$\gamma_{12}^{(c)} = \max_{pq, j \neq k} |\eta_p^j \eta_p^k \eta_q^k S_p(\omega_q)|.\quad (103)$$

For the 300  $\mu\text{s}$  test pulse both turned out to be very small. Thus,  $\hat{T}_{12}$  can be neglected.

The operator  $\hat{T}_{13}$  in (90) can be split into a diagonal part

$$\begin{aligned}\hat{T}_{13}^{(d)} &= \left(-\frac{1}{2}\right) \sum_{jpqr} (\eta_p^j)^2 \eta_q^j \eta_r^j [S_p(\omega_q + \omega_r) \hat{a}_q^\dagger \hat{a}_r^\dagger \\ &\quad + S_p(\omega_q - \omega_r) \hat{a}_q^\dagger \hat{a}_r + S_p^*(\omega_q - \omega_r) \hat{a}_q \hat{a}_r^\dagger + S_p^*(\omega_q + \omega_r) \hat{a}_q \hat{a}_r]\end{aligned}\quad (104)$$

and an off-diagonal part

$$\begin{aligned}\hat{T}_{13}^{(o)} &= \left(-\frac{1}{2}\right) \sum_{jkpqr} \hat{\sigma}_x^{(1)} \hat{\sigma}_x^{(2)} \eta_p^{(1)} \eta_p^{(2)} [\eta_q^{(1)} \eta_r^{(1)} + \eta_q^{(2)} \eta_r^{(2)}] [S_p(\omega_q + \omega_r) \hat{a}_q^\dagger \hat{a}_r^\dagger \\ &\quad + S_p(\omega_q - \omega_r) \hat{a}_q^\dagger \hat{a}_r + S_p^*(\omega_q - \omega_r) \hat{a}_q \hat{a}_r^\dagger + S_p^*(\omega_q + \omega_r) \hat{a}_q \hat{a}_r].\end{aligned}\quad (105)$$

The size of  $\hat{T}_{13}^{(d)}$  is controlled by

$$\gamma_{13}^{(d)} = \max_{\substack{j,pqr \\ \sigma = \pm 1}} |(\eta_p^j)^2 \eta_q^j \eta_r^j S_p(\omega_q + \sigma \omega_r)|.\quad (106)$$

For the 300  $\mu\text{s}$  test pulse we obtain

$$\gamma_{13}^{(d)} = 1.17 \times 10^{-3}. \quad (107)$$

Thus, compared to the target infidelity of  $\ll 10^{-4}$ , we cannot dismiss  $\hat{T}_{13}^{(d)}$  outright. However, taking  $\hat{T}_{13}^{(d)}$  as the error operator and since  $\hat{T}_{13}^{(d)}$  commutes with  $\sigma_x^{(1)}\sigma_x^{(2)}$ , we can use the infidelity estimate (35), which involves the squares of  $\hat{T}_{13}^{(d)}$ , i.e., the contribution of  $\hat{T}_{13}^{(d)}$  to the infidelity of  $\hat{U}(\tau)$  is expected to be of the order of  $(\gamma_{13}^{(d)})^2 \sim 10^{-6}$ . This means that the contribution of  $\hat{T}_{13}^{(d)}$  to the infidelity of  $\hat{U}(\tau)$  can be neglected.

We now turn to  $\hat{T}_{13}^{(o)}$ . It contains  $\sigma_x^{(1)}\sigma_x^{(2)}$  and thus contributes to over/under rotation of the XX gate, i.e., it contributes to  $\Delta\chi$  (see Table III). The operator  $\hat{T}_{13}^{(o)}$  acts in the computational space but also produces phonon excitations. However, according to (105), the two-phonon excitation terms are proportional to  $S_p(\omega_q + \omega_r)$ , which are nonresonant and very small. Assuming that the initial state starts out in the phonon ground state,  $|0\rangle_{\text{ph}}$ , the operator  $\hat{T}_{13}^{(o)}$  is, to an excellent approximation,

$$\hat{T}_{13}^{(o)} = \left(-\frac{1}{2}\right) \sum_{pq} \eta_p^{(1)}\eta_p^{(2)} [(\eta_q^{(1)})^2 + \eta_q^{(2)})^2] \sigma_x^{(1)}\sigma_x^{(2)} S_p(0). \quad (108)$$

Now, with (15),

$$\sum_p \eta_p^{(1)}\eta_p^{(2)} S_p(0) = \sum_p \eta_p^{(1)}\eta_p^{(2)} \int_0^\tau dt_1 \int_0^{t_1} dt_2 g(t_1)g(t_2) \sin[\omega_p(t_1 - t_2)] = \frac{\chi}{2}. \quad (109)$$

With this result,

$$\hat{T}_{13}^{(o)} = \left[ \left(-\frac{\chi}{4}\right) \sum_{jp} (\eta_p^j)^2 \right] \sigma_x^{(1)}\sigma_x^{(2)}. \quad (110)$$

The prefactor of the  $\sigma_x^{(1)}\sigma_x^{(2)}$  operator is a c-number. Therefore,  $\hat{T}_{13}^{(o)}$  produces a contribution to the degree of entanglement  $\chi$ . Since we have  $\hat{T}_{31} = \hat{T}_{13}$ , the total contribution to the degree of entanglement is

$$\Delta\chi = \left(-\frac{\chi}{2}\right) \sum_{jp} (\eta_p^j)^2. \quad (111)$$

Numerically, for the  $N = 7$  case (see Table II), we have

$$\sum_{jp} (\eta_p^j)^2 = 2.45 \times 10^{-2}. \quad (112)$$

For  $\chi = \pi/4$ , this results in

$$\Delta\chi = -9.62 \times 10^{-3}. \quad (113)$$

According to our numerical simulations (see Table III), we have  $\Delta\chi \approx -0.011$ . So, our analytical calculations predict the correct sign (under-rotation) of  $\chi$ . In addition, the magnitude of the relative error of our analytical prediction is  $(0.011 - 9.62 \times 10^{-3})/0.011 \approx 0.13$ , i.e., our analytical prediction is only of the order of 10% off.

According to (111),  $\Delta\chi$  depends only on the Lamb-Dicke parameters, and not on the gate duration  $\tau$ . This is reflected in Table III and explains why  $\Delta\chi$  in Table III is approximately constant, independent of  $\tau$ .

Summarizing the results obtained in this Section, we find that the second-order Magnus-expansion operators yield only two substantial contributions, i.e., the operator  $\hat{T}_{11}$ , which generates the desired XX gate and the operator  $2\hat{T}_{13}$  which explains the under-rotation of the gate angle and, approximately, its size, as listed in Table III.

At the end of Section VII, we noticed that  $\Delta\chi$  explains a significant contribution to the infidelity of  $\hat{U}(\tau)$ , but cannot explain the entire infidelity contribution. We took this as the motivation to look for the additional sources of infidelity in the various orders of the Magnus expansion. In this section we found that the second order explains only the origin of  $\Delta\chi$ , but does not reveal any additional significant sources of infidelity. Since the second order of the Magnus expansion did not reveal these sources, we now investigate the third order of the Magnus expansion, which, indeed, reveals the remaining significant sources of infidelity. In addition, we will find that this source of infidelity can be eliminated by the addition of a single linear equation to the control-pulse construction protocol.

### C. Third Order

In this section we compute  $\hat{W}_3(\tau)$ . With the definitions (66) stated at the end of the introduction to Section VIII, we have

$$\hat{W}_3(\tau) = \sum_{\alpha\beta\gamma=0}^4 \hat{T}_{\alpha\beta\gamma}. \quad (114)$$

All operators  $\hat{T}_{jkl}$  up to fourth order in  $\eta$  are listed in Section XVII (Appendix B). There is only a single operator of zeroth order in  $\eta$ , i.e.,  $\hat{T}_{000} \sim \eta^0$ . It is trivially zero and does not contribute to the infidelity.

There are three operators of first order in  $\eta$ , i.e.,  $\hat{T}_{001}$ ,  $\hat{T}_{010}$ ,  $\hat{T}_{100}$ , where [see Section XVII (Appendix B)]  $\hat{T}_{010} = 2\hat{T}_{001}$ , and  $\hat{T}_{100} = 0$ . This means that only  $\hat{T}_{001}$ 's contribution to the

infidelity has to be investigated. With (25), the infidelity caused by  $\hat{T}_{100}$  is controlled by

$$\gamma_{001} = \max_{jp} |\eta_p^j J_p|. \quad (115)$$

For the 300  $\mu\text{s}$  control pulse we obtain

$$\gamma_{001} = 1.2 \times 10^{-6}. \quad (116)$$

Therefore,  $\hat{T}_{001}$ , and with it  $\hat{T}_{010}$ , are negligible. Since  $\hat{T}_{100} = 0$ , all operators  $\sim \eta^1$  can be neglected.

There are six operators of second order in  $\eta$ , i.e.,  $\hat{T}_{002}$ ,  $\hat{T}_{011}$ ,  $\hat{T}_{020}$ ,  $\hat{T}_{101}$ ,  $\hat{T}_{110}$ , and  $\hat{T}_{200}$ . Of these, according to Section XVII, only  $\hat{T}_{011}$ ,  $\hat{T}_{101}$ , and  $\hat{T}_{110}$  are nonzero, and of those, only  $\hat{T}_{011}$  and  $\hat{T}_{110}$  are non-negligible. While  $\hat{T}_{011}$  acts only on the computational space,  $\hat{T}_{110}$  also has a part that produces phonon excitations. This part, however, is negligibly small. As an overall result of the operators  $\sim \eta^2$ , we obtain that the effective error operator corresponding to the leading parts of  $\hat{T}_{011}$  and  $\hat{T}_{110}$  is

$$\hat{E}^{\sigma_x \sigma_z} = 4\Phi[\eta, g] [\hat{\sigma}_x^{(1)} \hat{\sigma}_z^{(2)} + \hat{\sigma}_x^{(2)} \hat{\sigma}_z^{(1)}]. \quad (117)$$

We checked that all operators of order three and four in  $\eta$  are negligible. Thus, (117) is the only significant error operator that results from the third-order Magnus expansion. We note that this operator acts only in the computational space, not in the phonon space. With (50) and  $\lambda = 4\Phi[\eta, g]$ , we obtain for the infidelity contribution of (117) for  $|\psi_0\rangle = |00\rangle|0\rangle_{\text{ph}}$ :

$$\bar{F}_S^{(\sigma_x \sigma_z)} = \left( \frac{\lambda \sin(\chi)}{\chi} \right)^2 \langle \psi_0 | [\sigma_x^{(1)} \sigma_z^{(2)} + \sigma_x^{(2)} \sigma_z^{(1)}]^2 | \psi_0 \rangle = \left( \frac{4\lambda}{\pi} \right)^2. \quad (118)$$

For the 300  $\mu\text{s}$  test pulse we have

$$\lambda = 1.17 \times 10^{-2}. \quad (119)$$

Thus, with (118) we obtain:

$$\bar{F}_S^{(\sigma_x \sigma_z)} = 2.2 \times 10^{-4}. \quad (120)$$

Together with (113), we now obtain an estimate for the total infidelity of the 300  $\mu\text{s}$  test pulse according to

$$\bar{F}_S = (\Delta\chi)^2 + \bar{F}_S^{(\sigma_x \sigma_z)} = (-9.62 \times 10^{-3})^2 + 2.2 \times 10^{-4} = 3.1 \times 10^{-4}. \quad (121)$$

According to Table III, this accounts for about 80% of the infidelity of the 300  $\mu\text{s}$  test pulse. Since, via calibration,  $\Delta\chi$  can always be set to zero, generating control pulses that zero out

the  $\Phi$  functional may go a long way to reduce the infidelity. How to generate such control pulses, and that this recipe actually works to suppress the the infidelity below  $10^{-4}$ , is shown in the following section.

## IX. IMPROVED CONTROL-PULSE CONSTRUCTION

In Section VII we argued, and proved numerically, that a significant portion of the infidelity can be removed by calibration of the control pulse. Here we show that by eliminating the infidelity due to the  $\Phi$ -functional (see Section VIII C), we can further suppress the infidelity below the level of  $10^{-4}$ . To eliminate  $\Phi$ , we add the single linear equation

$$\sum_n \frac{B_n}{n} = 0 \quad (122)$$

to the AMFM pulse-solver code and obtain new pulses  $\tilde{g}(t)$  that zero out  $\Phi[\eta, \tilde{g}]$ , defined in (27). That the AMFM code with the condition (122) added produces control pulses  $\tilde{g}(t)$  with  $\Phi[\eta, \tilde{g}] = 0$  was confirmed explicitly. As discribed in Section VII,  $\tilde{g}(t)$  may be renormalized (calibrated) such that  $\tilde{g}(t)$  not only produces  $\Phi[\eta, \tilde{g}] = 0$ , but simultaneously produces  $\Delta\chi = 0$ . Running our gate-simulator code (see Section IV) with the calibrated pulses  $\tilde{g}(t)$ , we obtain the infidelities  $\bar{F}_S^{\Phi,c}$ ,  $\bar{F}_G^{\Phi,c}$ , and  $\bar{F}_\Phi^{\Phi,c}$  as shown in Table III. We see that in all cases the calibrated pulses  $\tilde{g}(t)$  produce infidelities below  $10^{-4}$ . We note that the calibrated pulses  $\tilde{g}(t)$  require only insignificantly larger power compared with the original pulses  $g(t)$ . This is as expected, since only one additional condition, i.e., the condition (122), was added to the original set of linear phase-space closure conditions (14). We point out that, in conjunction with calibration, the construction of the improved AMFM pulses is still a *linear* process. Nonlinear optimizer codes are not required.

## X. SCALING

So far we have focused entirely on the 7-ion case for which we have a complete analysis machinery in place consisting of pulse construction, analytical formulas for error estimates, and a gate simulator that includes all the relevant phonon states (see Section IV). But how do the control errors scale with the number of ions  $N$ ? Since the required pulse power increases with increasing  $N$  [23] but at the same time the Lamb-Dicke parameters  $\eta$  decrease, this is

an open question. We partially answer this question in the following way. Our analytical results do not depend on the number of ions  $N$  in the chain, i.e., our analytical results are valid for any number of qubits. In particular, as soon as a control pulse is generated (it does not matter whether this is an AM pulse, FM pulse, AMFM pulse, or any other type of pulse), this pulse can immediately be inserted into our analytical formulas, which then may be used to obtain infidelity estimates for this particular  $N$ -ion control pulse. We illustrate this method for  $N = 36$  by computing the infidelity (118), i.e., the leading source of infidelity, for  $N = 36$  uncalibrated control pulses for 2-qubit XX gates between all possible gate combinations  $(i_0, j_0)$ ,  $j_0 = 1, \dots, i_0 - 1$ ,  $i_0 = 2, \dots, 36$ . This results in 630 gate combinations. The infidelities obtained are displayed in Fig. 2 in the form of a bar graph, where the height of a bar shows the frequency of occurrence of infidelities within the width of the bar. The infidelities in Fig. 2 are in units of  $10^{-4} = 1$  pptt, where the unit ‘‘pptt’’ denotes one part per ten thousand. We see that the infidelities generated by  $N = 36$  control pulses constructed on the basis of the Standard Hamiltonian  $\hat{H}_S$  are significant, and in many cases they are much larger than 10 pptt. This particular error source, in conjunction with calibration, can now be eliminated completely by using the linear construction technique outlined in Section IX. The histogram in Fig. 2 was made for  $300 \mu\text{s}$  AMFM pulses. The question is: How does this scale with the gate time  $\tau$ . To answer this question, we also computed 36-ion AMFM histograms at  $700 \mu\text{s}$ . The result is that most of the  $\Phi$ -infidelities for the  $700 \mu\text{s}$  AMFM histogram are below 5 pptt. About half of the gates are good gates with infidelities less than 1 pptt and most of the other gates have  $\Phi$ -infidelities less than 5 pptt. This indicates that the  $\Phi$ -infidelity is a sensitive function of gate time  $\tau$ .

## XI. DISCUSSION

In this paper we consider neither stochastic nor systematic errors in the quantum computer hardware. Instead, we ask a different question: Even in the absence of all stochastic and systematic hardware errors, i.e., even in the ideal situation that the quantum computer is governed exactly by the model Hamiltonian  $\hat{H}_M$  (see Fig. FIG-1 and discussion in Section I), and given that the pulse construction is based on the Standard Hamiltonian  $\hat{H}_S$ , is it even in principle possible in this idealized case to reach XX gate infidelities better than  $10^{-4}$  for all gates? The answer given in this paper (see, in particular, Table III and Fig. 2),

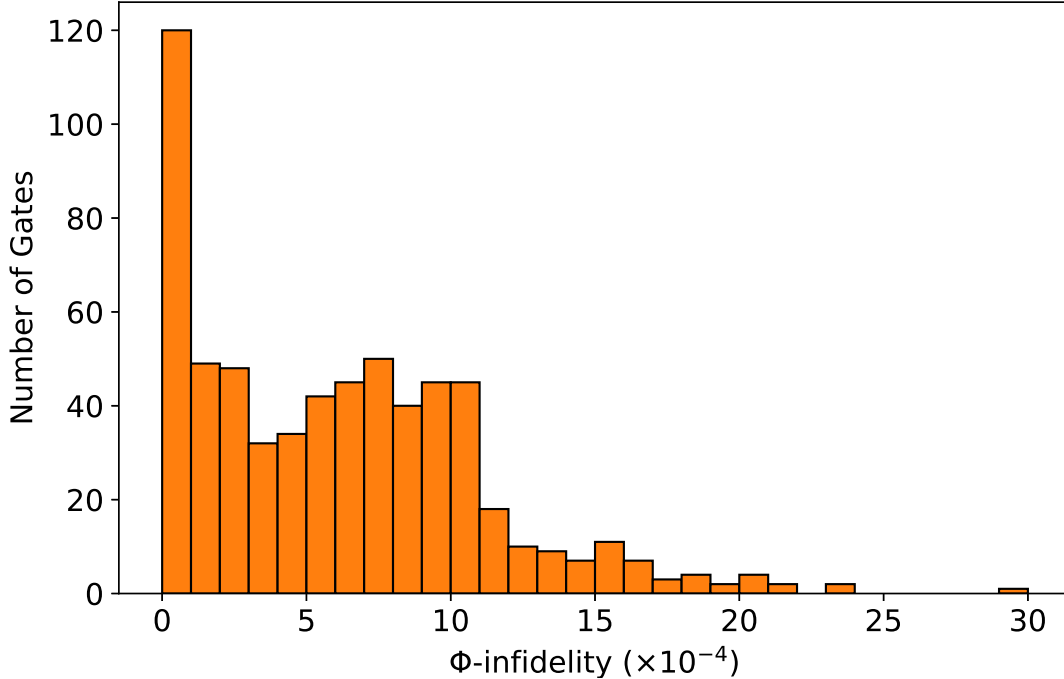


FIG. 2. Number of gates vs.  $\Phi$ -infidelity for  $N = 36$ -ions, uncalibrated,  $\tau = 300 \mu\text{s}$  AMFM pulses, not requiring the  $\Phi$  condition (122). The infidelities are in units of  $10^{-4}$ . The histogram plot illustrates that given a  $10^{-4}$  fidelity target, the infidelities introduced by control pulses not requiring (122) are severe for a majority of  $N = 36$  gates. Conversely, requiring (122), a single, linear equation added to the pulse-construction protocol, eliminates this type of infidelity completely.

is no. However, we also show that by slightly modifying the pulse construction protocol by including only the single additional linear condition (122), and subsequently calibrating the pulse obtained, it is possible to eliminate the two leading sources of infidelity and, at least in the 7-ion case considered in detail in this paper, then achieve infidelities smaller than  $10^{-4}$  in all cases considered. While, in Section X, we demonstrated that the coherent errors produced by the error operator (117) persist even in the  $N = 36$  case, due to limited computer resources, we are not currently able to show that, following the new pulse-construction protocol, the infidelity can be suppressed below  $10^{-4}$  in this case as well. However, as an application of our analytical formulas stated in Sections VIII A, VIII B, VIII C, and XVII (Appendix B), we are confident that even in the  $N = 36$  case our two-stage protocol of pulse construction, i.e., implementing (122) with subsequent calibration (see Section VII),

will result in pulses that produce infidelities smaller than  $10^{-4}$ .

## XII. SUMMARY AND CONCLUSIONS

In this paper, focusing on the phase-sensitive geometry [24], we found that even in the absence of all experimental coherent and incoherent errors, the control pulses  $g(t)$  computed on the basis of the Standard Hamiltonian  $\hat{H}_S$  are not accurate enough to consistently generate XX gates with infidelities  $\lesssim 10^{-4}$ . For ion chains consisting of  $N = 7$  ions (7-qubit case), we based this conclusion on numerical simulations including all relevant phonon states, and on analytical evaluations of error terms generated by a third-order Magnus expansion, keeping all commutator terms up to fourth order in the Lamb-Dicke parameters  $\eta$ . Not satisfied with this negative result, identifying the two leading sources of coherent errors we defined a new control-pulse construction protocol obtained by adding a single, *linear* equation to the standard phase-space closure equations that eliminates both  $\Delta\chi$  and  $\Phi$  errors. In all  $N = 7$ -cases studied in this paper, pulses generated with the new pulse-construction protocol produced XX-gate infidelities  $\lesssim 10^{-4}$ . We also showed that increasing the number of ions in the chain to  $N = 36$ , the two principal sources of coherent control errors remain. While our computational resources are not currently sufficient to run our gate simulator code for the  $N = 36$  case, we are confident that even in this case, our two-stage method of zeroing out the  $\Phi$  functional (27) [i.e., adding the linear equation (122)] with subsequent calibration of the pulse (see Section VII) will suppress the infidelity substantially toward or below  $\lesssim 10^{-4}$ .

## XIII. AUTHOR CONTRIBUTIONS

All authors participated in the framing and discussion of the project and the evaluation of the results. R.B. performed all analytical and numerical calculations. All authors participated in the writing of the paper.

## XIV. DATA AVAILABILITY

Data and codes underlying this work are available from the corresponding author upon reasonable request.



## XV. CONFLICTS OF INTEREST

The authors declare no conflicts of interest.

## XVI. APPENDIX A: GATE SIMULATOR MATRIX ELEMENTS

In this section we present the matrix elements of the full Hamiltonian  $\hat{H}_{MS}$  as well as the ones of the model Hamiltonians  $\hat{H}^{(N_c, N_s)}$ . We start with the matrix elements of the full Hamiltonian,  $\hat{H}_{MS}$ .

The matrix elements of the cosine part of  $\hat{H}_{MS}$  are

$$\begin{aligned}
C_{n_1 n_2 \dots; m_1 m_2 \dots}^{(j)} &= \langle n_1 n_2 \dots | \cos \left[ \sum_p \eta_p^j (\hat{a}_p^\dagger + \hat{a}_p) \right] | m_1 m_2 \dots \rangle \\
&= \frac{1}{2} \langle n_1 n_2 \dots | e^{i \sum_p \eta_p^j (\hat{a}_p^\dagger + \hat{a}_p)} + e^{-i \sum_p \eta_p^j (\hat{a}_p^\dagger + \hat{a}_p)} | m_1 m_2 \dots \rangle \\
&= \frac{1}{2} \left\{ \prod_p \langle n_p | e^{i \eta_p^j (\hat{a}_p^\dagger + \hat{a}_p)} | m_p \rangle + \prod_p \langle n_p | e^{-i \eta_p^j (\hat{a}_p^\dagger + \hat{a}_p)} | m_p \rangle \right\}. \tag{123}
\end{aligned}$$

We see that  $C_{n_1 n_2 \dots; m_1 m_2 \dots}^{(j)}$  is real and symmetric in  $n_p \leftrightarrow m_p$ . Thus, we can arrange for  $n_p \geq m_p$  for all  $p$ . With  $n_p \geq m_p$  and

$$\langle n | e^{\lambda \hat{a}^\dagger} | m \rangle = \begin{cases} 0 & \text{if } m > n \\ \frac{\lambda^{n-m}}{(n-m)!} \left[ \frac{n!}{m!} \right]^{1/2} & \text{if } m \leq n. \end{cases} \tag{124}$$

we have

$$\begin{aligned}
C_{n_1 n_2 \dots; m_1 m_2 \dots}^{(j)} &= \frac{1}{2} \prod_p e^{-(\eta_p^j)^2 / 2} \left( \frac{m_p!}{n_p!} \right)^{1/2} (\eta_p^j)^{n_p - m_p} L_{m_p}^{(n_p - m_p)} [(\eta_p^j)^2] \\
&\quad \left\{ \prod_p i^{(n_p - m_p)} + \prod_p (-i)^{(n_p - m_p)} \right\}. \tag{125}
\end{aligned}$$

Now, define

$$\sigma = \left[ \sum_p (n_p - m_p) \right] \text{ mod } 4. \tag{126}$$

Then:

$$C_{n_1 n_2 \dots; m_1 m_2 \dots}^{(j)} = \prod_p e^{-(\eta_p^j)^2/2} \left( \frac{m_p!}{n_p!} \right)^{1/2} (\eta_p^j)^{n_p - m_p} L_{m_p}^{(n_p - m_p)} [(\eta_p^j)^2] \begin{cases} 1, & \text{if } \sigma = 0, \\ 0, & \text{if } \sigma = 1, \\ -1, & \text{if } \sigma = 2, \\ 0, & \text{if } \sigma = 3. \end{cases} \quad (127)$$

Because of

$$C_{n_1 n_2 \dots; m_1 m_2 \dots}^{(j)} \sim \prod_p (\eta_p^j)^{n_p - m_p}, \quad (128)$$

and  $|\eta_p^j| \ll 1$ , we see that  $C_{n_1 n_2 \dots; m_1 m_2 \dots}^{(j)}$  is very close to diagonal, i.e., only the first few off-diagonals are significantly different from zero. This fact can be used to speed up the numerical integration of the system of linear equations significantly.

Similarly, we obtain

$$\begin{aligned} S_{n_1 n_2 \dots; m_1 m_2 \dots}^{(j)} &= \langle n_1 n_2 \dots | \sin \left[ \sum_p \eta_p^j (\hat{a}_p^\dagger + \hat{a}_p) \right] | m_1 m_2 \dots \rangle \\ &= \prod_p e^{-(\eta_p^j)^2/2} \left( \frac{m_p!}{n_p!} \right)^{1/2} (\eta_p^j)^{n_p - m_p} L_{m_p}^{(n_p - m_p)} [(\eta_p^j)^2] \begin{cases} 0, & \text{if } \sigma = 0, \\ 1, & \text{if } \sigma = 1, \\ 0, & \text{if } \sigma = 2, \\ -1, & \text{if } \sigma = 3. \end{cases} \end{aligned} \quad (129)$$

## XVII. APPENDIX B: THIRD-ORDER COMMUTATORS

In this appendix we list the results of all third-order commutators  $T_{\alpha\beta\gamma}$  as defined in (66) with  $\eta$  orders  $\eta^m$ ,  $m \leq 4$ . We group the commutators according to their  $\eta$  order  $m$ .

Commutators  $\hat{T}_{\alpha\beta\gamma} \sim \eta^0$ :

$$\hat{T}_{000} = 0, \quad (130)$$

Commutators  $\hat{T}_{\alpha\beta\gamma} \sim \eta^1$ :

$$\hat{T}_{001} = \left( \frac{2}{3} \right) \sum_{j=1,2} \left[ \int_0^\tau g(t) G^2(t) \hat{V}_j(t) dt \right] \hat{\sigma}_x^{(j)}, \quad (131)$$

$$\hat{T}_{010} = 2\hat{T}_{001}, \quad (132)$$

$$\hat{T}_{100} = 0, \quad (133)$$

Commutators  $\hat{T}_{\alpha\beta\gamma} \sim \eta^2$ :

$$\hat{T}_{002} = 0, \quad (134)$$

$$\hat{T}_{011} = \left(\frac{8}{3}\right) \Phi[\eta, g] [\hat{\sigma}_x^{(1)} \hat{\sigma}_z^{(2)} + \hat{\sigma}_x^{(2)} \hat{\sigma}_z^{(1)}], \quad (135)$$

$$\hat{T}_{020} = 0, \quad (136)$$

$$\begin{aligned} \hat{T}_{101} &= \left(-\frac{2}{3}\right) \sum_{j=1,2} \hat{\sigma}_y^{(j)} \int_0^\tau dt_1 \int_0^{t_1} dt_2 g(t_1) g(t_2) \\ &\quad [G(t_1) - G(t_2)] [\hat{V}_j(t_1) \hat{V}_j(t_2) + \hat{V}_j(t_2) \hat{V}_j(t_1)], \end{aligned} \quad (137)$$

$$\begin{aligned} \hat{T}_{110} &= \left(-\frac{2}{3}\right) \int_0^\tau dt_1 \int_0^{t_1} dt_2 g(t_1) g(t_2) G(t_1) \\ &\quad \sum_j [\hat{V}_j(t_1) \hat{V}_j(t_2) + \hat{V}_j(t_2) \hat{V}_j(t_1)] \hat{\sigma}_y^{(j)} \\ &\quad + \left(\frac{4}{3}\right) \Phi[\eta, g] [\hat{\sigma}_x^{(1)} \hat{\sigma}_z^{(2)} + \hat{\sigma}_x^{(2)} \hat{\sigma}_z^{(1)}], \end{aligned} \quad (138)$$

$$\hat{T}_{200} = 0. \quad (139)$$

Commutators  $\hat{T}_{\alpha\beta\gamma} \sim \eta^3$ :

$$\hat{T}_{003} = \left(-\frac{1}{9}\right) \sum_j \left\{ \int_0^\tau g(t) G^2(t) \hat{V}_j^3(t) dt \right\} \hat{\sigma}_x^{(j)}, \quad (140)$$

$$\begin{aligned} \hat{T}_{012} &= \left(\frac{1}{6}\right) \sum_k \hat{\sigma}_x^{(k)} \int_0^\tau dt_1 \int_0^{t_1} dt_2 g(t_1) g(t_2) \\ &\quad \left\{ G(t_2) [\hat{V}_k(t_2) \hat{V}_k^2(t_1) + \hat{V}_k^2(t_1) \hat{V}_k(t_2)] \right. \\ &\quad \left. - G(t_1) [\hat{V}_k(t_1) \hat{V}_k^2(t_2) + \hat{V}_k^2(t_2) \hat{V}_k(t_1)] \right\} \\ &\quad - \left(\frac{2}{3}\right) \sum_p \eta_p^1 \eta_p^2 \int_0^\tau dt_1 \int_0^{t_1} dt_2 g(t_1) g(t_2) \sin[\omega_p(t_1 - t_2)] \\ &\quad \left\{ [G(t_2) \hat{V}_1(t_1) + G(t_1) \hat{V}_1(t_2)] \hat{\sigma}_y^{(1)} \hat{\sigma}_z^{(2)} \right. \\ &\quad \left. + [G(t_2) \hat{V}_2(t_1) + G(t_1) \hat{V}_2(t_2)] \hat{\sigma}_y^{(2)} \hat{\sigma}_z^{(1)} \right\}, \end{aligned} \quad (141)$$

$$\begin{aligned}
\hat{T}_{021} &= \left(\frac{1}{3}\right) \sum_k \hat{\sigma}_x^{(k)} \int_0^\tau dt_1 \int_0^{t_1} dt_2 g(t_1)g(t_2)G(t_1) \\
&\quad [\hat{V}_k^2(t_1)\hat{V}_k(t_2) + \hat{V}_k(t_2)\hat{V}_k^2(t_1)] \\
&\quad - \left(\frac{2}{3}\right) \sum_p \eta_p^1 \eta_p^2 \int_0^\tau dt_1 \int_0^{t_1} dt_2 g(t_1)g(t_2) \sin[\omega_p(t_1 - t_2)] \\
&\quad \left\{ [G(t_2)\hat{V}_1(t_2) + G(t_1)\hat{V}_1(t_1)]\hat{\sigma}_y^{(1)}\hat{\sigma}_z^{(2)} \right. \\
&\quad \left. + [G(t_2)\hat{V}_2(t_2) + G(t_1)\hat{V}_2(t_1)]\hat{\sigma}_y^{(2)}\hat{\sigma}_z^{(1)} \right\}, \tag{142}
\end{aligned}$$

$$\hat{T}_{030} = \left(-\frac{2}{9}\right) \sum_{j=1,2} \hat{\sigma}_x^{(j)} \int_0^\tau g(t)G^2(t)\hat{V}_j^3(t) dt, \tag{143}$$

$$\hat{T}_{102} = 0, \tag{144}$$

$$\hat{T}_{111} = 0, \tag{145}$$

$$\hat{T}_{120} = 0, \tag{146}$$

$$\begin{aligned}
\hat{T}_{201} &= \left(-\frac{1}{6}\right) \sum_j \hat{\sigma}_x^{(j)} \int_0^\tau dt_1 \int_0^{t_1} dt_2 g(t_1)g(t_2)[G(t_1) - G(t_2)] \\
&\quad \left\{ \hat{V}_j^2(t_1)\hat{V}_j(t_2) + \hat{V}_j(t_2)\hat{V}_j^2(t_1) + \hat{V}_j^2(t_2)\hat{V}_j(t_1) + \hat{V}_j(t_1)\hat{V}_j^2(t_2) \right\} \\
&\quad + \left(\frac{2}{3}\right) \sum_{p,j \neq k} \hat{\sigma}_y^{(j)}\hat{\sigma}_z^{(k)} \eta_p^j \eta_p^k \\
&\quad \int_0^\tau dt_1 \int_0^{t_1} dt_2 g(t_1)g(t_2)[G(t_1) - G(t_2)] \sin[\omega_p(t_1 - t_2)] [\hat{V}_j(t_1) - \hat{V}_j(t_2)], \tag{147}
\end{aligned}$$

$$\begin{aligned}
\hat{T}_{210} &= \left(\frac{1}{6}\right) \sum_j \hat{\sigma}_x^{(j)} \int_0^\tau dt_1 \int_0^{t_1} dt_2 g(t_1)g(t_2) \\
&\quad \left\{ G(t_2)[\hat{V}_j^2(t_1)\hat{V}_j(t_2) + \hat{V}_j(t_2)\hat{V}_j^2(t_1)] - G(t_1)[\hat{V}_j^2(t_2)\hat{V}_j(t_1) + \hat{V}_j(t_1)\hat{V}_j^2(t_2)] \right\} \\
&\quad - \left(\frac{2}{3}\right) \sum_{p,j \neq k} \hat{\sigma}_y^{(j)}\hat{\sigma}_z^{(k)} \eta_p^j \eta_p^k \int_0^\tau dt_1 \int_0^{t_1} dt_2 g(t_1)g(t_2) \sin[\omega_p(t_1 - t_2)] \\
&\quad [G(t_2)\hat{V}_j(t_1) + G(t_1)\hat{V}_j(t_2)], \tag{148}
\end{aligned}$$

$$\hat{T}_{300} = 0. \tag{149}$$

Commutators  $\hat{T}_{\alpha\beta\gamma} \sim \eta^4$ :

$$\hat{T}_{004} = 0, \tag{150}$$

$$\begin{aligned}
\hat{T}_{013} &= \left(-\frac{1}{3}\right) [\hat{\sigma}_x^{(1)}\hat{\sigma}_z^{(2)} + \hat{\sigma}_x^{(2)}\hat{\sigma}_z^{(1)}] \\
&\quad \sum_{p,j=1,2} \eta_p^1 \eta_p^2 \int_0^\tau dt_1 \int_0^{t_1} dt_2 g(t_1)g(t_2) \sin[\omega_p(t_1 - t_2)] \\
&\quad [G(t_1)\hat{V}_j^2(t_2) + G(t_2)\hat{V}_j^2(t_1)], \tag{151}
\end{aligned}$$

$$\hat{T}_{022} = 0, \tag{152}$$

$$\begin{aligned}
\hat{T}_{031} &= \left(-\frac{2}{3}\right) [\hat{\sigma}_x^{(1)}\hat{\sigma}_z^{(2)} + \hat{\sigma}_x^{(2)}\hat{\sigma}_z^{(1)}] \\
&\quad \sum_{p,j=1,2} \eta_p^1 \eta_p^2 \int_0^\tau dt_1 \int_0^{t_1} dt_2 g(t_1)g(t_2)G(t_1) \sin[\omega_p(t_1 - t_2)]\hat{V}_j^2(t_1), \tag{153}
\end{aligned}$$

$$\hat{T}_{040} = 0, \tag{154}$$

$$\begin{aligned}
\hat{T}_{103} &= \int_0^\tau dt_1 \int_0^{t_1} dt_2 g(t_1)g(t_2)[G(t_1) - G(t_2)] \\
&\quad \left\{ \left(\frac{1}{18}\right) \sum_{j=1,2} \hat{\sigma}_y^{(j)} [\hat{V}_j(t_1)\hat{V}_j^3(t_2) + \hat{V}_j^3(t_2)\hat{V}_j(t_1) + \hat{V}_j(t_2)\hat{V}_j^3(t_1) + \hat{V}_j^3(t_1)\hat{V}_j(t_2)] \right. \\
&\quad \left. + \left(\frac{1}{3}\right) \sum_{j \neq k} \hat{\sigma}_x^{(j)}\hat{\sigma}_z^{(k)} \sum_p \eta_p^j \eta_p^k [\hat{V}_k^2(t_2) - \hat{V}_k^2(t_1)] \sin[\omega_p(t_1 - t_2)] \right\}, \tag{155}
\end{aligned}$$

$$\begin{aligned}
\hat{T}_{112} = & \left(\frac{1}{6}\right) \int_0^\tau dt_1 \int_0^{t_1} dt_2 \int_0^{t_2} dt_3 g(t_1)g(t_2)g(t_3) \\
& \left\{ \left(-\frac{1}{2}\right) \sum_j \hat{\sigma}_y^{(j)} \left\{ \hat{V}_j(t_1) [\hat{V}_j(t_2) \hat{V}_j^2(t_3) + \hat{V}_j^2(t_3) \hat{V}_j(t_2)] \right. \right. \\
& + [\hat{V}_j(t_2) \hat{V}_j^2(t_3) + \hat{V}_j^2(t_3) \hat{V}_j(t_2)] \hat{V}_j(t_1) + \hat{V}_j(t_3) [\hat{V}_j(t_2) \hat{V}_j^2(t_1) + \hat{V}_j^2(t_1) \hat{V}_j(t_2)] \\
& + [\hat{V}_j(t_2) \hat{V}_j^2(t_1) + \hat{V}_j^2(t_1) \hat{V}_j(t_2)] \hat{V}_j(t_3) \left. \right\} \\
& - 2 \sum_{p,j \neq k} \hat{\sigma}_x^{(j)} \hat{\sigma}_z^{(k)} \eta_p^j \eta_p^k \\
& \left\{ \hat{V}_k^2(t_3) \sin[\omega_p(t_1 - t_2)] - V_k^2(t_1) \sin[\omega_p(t_2 - t_3)] \right. \\
& + [\hat{V}_k(t_2) \hat{V}_k(t_3) + \hat{V}_k(t_3) \hat{V}_k(t_2)] \sin[\omega_p(t_1 - t_3)] \\
& - [\hat{V}_k(t_2) \hat{V}_k(t_1) + \hat{V}_k(t_1) \hat{V}_k(t_2)] \sin[\omega_p(t_1 - t_3)] \left. \right\} \\
& + 4 \sum_{pq} \eta_p^1 \eta_p^2 \eta_q^1 \eta_q^2 (\hat{\sigma}_y^{(1)} + \hat{\sigma}_y^{(2)}) \sin[\omega_q(t_1 - t_3)] \\
& \{ \sin[\omega_p(t_2 - t_3)] - \sin[\omega_p(t_2 - t_1)] \} \\
& - 2 \sum_p \eta_p^1 \eta_p^2 \hat{\sigma}_x^{(1)} \hat{\sigma}_z^{(2)} [\hat{V}_2(t_1) \hat{V}_2(t_3) + \hat{V}_2(t_3) \hat{V}_2(t_1)] \\
& \{ \sin[\omega_p(t_2 - t_3)] + \sin[\omega_p(t_2 - t_1)] \} \\
& - 2 \sum_p \eta_p^1 \eta_p^2 \hat{\sigma}_x^{(2)} \hat{\sigma}_z^{(1)} [\hat{V}_1(t_1) \hat{V}_1(t_3) + \hat{V}_1(t_3) \hat{V}_1(t_1)] \\
& \left. \{ \sin[\omega_p(t_2 - t_3)] + \sin[\omega_p(t_2 - t_1)] \} \right\}, \tag{156}
\end{aligned}$$

$$\begin{aligned}
\hat{T}_{121} = & \left(-\frac{1}{12}\right) \int_0^\tau dt_1 \int_0^{t_1} dt_2 \int_0^{t_2} dt_3 g(t_1)g(t_2)g(t_3) \\
& \sum_{jkl} \left\{ 2[\hat{V}_j(t_1) \hat{V}_k^2(t_2) \hat{V}_l(t_3) + \hat{V}_j(t_3) \hat{V}_k^2(t_2) \hat{V}_l(t_1)] \hat{\sigma}_x^{(j)} \hat{\sigma}_y^{(k)} \hat{\sigma}_x^{(l)} \right. \\
& - [\hat{V}_j(t_1) \hat{V}_k(t_3) \hat{V}_l^2(t_2) + \hat{V}_j(t_3) \hat{V}_k(t_1) \hat{V}_l^2(t_2)] \hat{\sigma}_x^{(j)} \hat{\sigma}_x^{(k)} \hat{\sigma}_y^{(l)} \\
& \left. - [\hat{V}_j^2(t_2) \hat{V}_k(t_3) \hat{V}_l(t_1) + \hat{V}_j^2(t_2) \hat{V}_k(t_1) \hat{V}_l(t_3)] \hat{\sigma}_y^{(j)} \hat{\sigma}_x^{(k)} \hat{\sigma}_x^{(l)} \right\}, \tag{157}
\end{aligned}$$

$$\begin{aligned}
\hat{T}_{130} &= \left(\frac{1}{9}\right) \int_0^\tau dt_1 \int_0^{t_1} dt_2 g(t_1)g(t_2)G(t_1) \\
&\quad \left\{ \sum_{j=1,2} \sigma_y^{(j)} [\hat{V}_j(t_2)\hat{V}_j^3(t_1) + \hat{V}_j^3(t_1)\hat{V}_j(t_2)] \right\} \\
&\quad - \left(\frac{2}{3}\right) \int_0^\tau dt_1 \int_0^{t_1} dt_2 g(t_1)g(t_2) \\
&\quad \sum_{\substack{j,k=1,2 \\ j \neq k}}^N \sum_{p=1} \eta_p^j \eta_p^k \sigma_x^j \sigma_z^k G(t_1) \hat{V}_k^2(t_1) \sin[\omega_p(t_1 - t_2)], \tag{158}
\end{aligned}$$

$$\hat{T}_{202} = 0 \tag{159}$$

$$\begin{aligned}
\hat{T}_{211} &= \left(\frac{4}{3}\right) \sum_{p,k \neq j} \eta_p^1 \eta_p^2 \hat{\sigma}_z^{(j)} \hat{\sigma}_x^{(k)} \\
&\quad \int_0^\tau dt_1 \int_0^{t_1} dt_2 \int_0^{t_2} dt_3 g(t_1)g(t_2)g(t_3) \hat{V}_j^2(t_1) \sin[\omega_p(t_2 - t_3)], \tag{160}
\end{aligned}$$

$$\hat{T}_{220} = 0, \tag{161}$$

$$\begin{aligned}
\hat{T}_{301} &= \left(\frac{1}{18}\right) \int_0^\tau dt_1 \int_0^{t_1} dt_2 g(t_1)g(t_2)[G(t_1) - G(t_2)] \\
&\quad \left\{ \sum_{j=1,2} \sigma_y^{(j)} [V_j^3(t_1)V_j(t_2) + V_j(t_2)V_j^3(t_1) + V_j^3(t_2)V_j(t_1) + V_j(t_1)V_j^3(t_2)] \right\} \\
&\quad + \left(\frac{1}{3}\right) \int_0^\tau dt_1 \int_0^{t_1} dt_2 g(t_1)g(t_2)[G(t_1) - G(t_2)] \\
&\quad \sum_{\substack{j,k=1,2 \\ j \neq k}}^N \sum_{p=1} \eta_p^j \eta_p^k \sigma_x^j \sigma_z^k [\hat{V}_j^2(t_1) - \hat{V}_j^2(t_2)] \sin[\omega_p(t_1 - t_2)], \tag{162}
\end{aligned}$$

$$\begin{aligned}
\hat{T}_{310} &= \left(\frac{1}{18}\right) \int_0^\tau dt_1 \int_0^{t_1} dt_2 g(t_1)g(t_2) \\
&\quad \left[ \sum_{j=1,2} \hat{\sigma}_y^{(j)} \left\{ G(t_1) [\hat{V}_j^3(t_2)\hat{V}_j(t_1) + \hat{V}_j(t_1)\hat{V}_j^3(t_2)] \right. \right. \\
&\quad \left. \left. - G(t_2) [\hat{V}_j^3(t_1)\hat{V}_j(t_2) + \hat{V}_j(t_2)\hat{V}_j^3(t_1)] \right\} \right] \\
&\quad - \left(\frac{1}{3}\right) \int_0^\tau dt_1 \int_0^{t_1} dt_2 g(t_1)g(t_2) \sin[\omega_p(t_1 - t_2)] \\
&\quad \sum_{\substack{j,k=1,2 \\ j \neq k}}^N \sum_{p=1} \eta_p^j \eta_p^k \sigma_x^j \sigma_z^k [G(t_1)\hat{V}_j^2(t_2) + G(t_2)\hat{V}_j^2(t_1)]. \tag{163}
\end{aligned}$$

$$\hat{T}_{400} = 0. \tag{164}$$

- 
- [1] M. A. Nielsen and I. L. Chuang, *Quantum Computation and Quantum Information* (Cambridge University Press, Cambridge, 2000).
- [2] C. T., S. Debnath, T. A. Manning, C. Figgatt, Z.-X. Gong, L.-M. Duan, and C. Monroe, *Phys. Rev. Lett.* **112**, 190502 (2014).
- [3] K. Wright, K. M. Beck, S. Debnath, J. M. Amini, Y. Nam, N. Grzesiak, J.-S. Chen, N. C. Pimenti, M. Chmielewski, C. Collins<sup>1</sup>, K. M. Hudek, J. Mizrahi<sup>1</sup>, J. D. Wong-Campos, S. Allen, J. Apisdorf, P. Solomon, M. Williams, A. M. DuCore, A. Blinov, S. M. Kreikemeier, V. Chaplin, M. Keesan, C. Monroe, and J. Kim, *Nature Communications* **10**, 5464 (2019).
- [4] S.-L. Zhu, C. Monroe, and L.-M. Duan, *Europhys. Lett.* **73**, 485 (2006).
- [5] N. M. Linke, D. Maslov, M. Roetteler, S. Debnath, C. Figgatt, K. A. Landsman, K. Wright, and C. Monroe, *Proc. Natl. Acad. Sci. U.S.A.* **114**, 3305 (2017).
- [6] P. Wang, C.-Y. Luan, M. Qiao, M. Um, J. Zhang, Y. Wang, X. Yuan, M. Gu, J. Zhang, and K. Kim, *Nature Communications* **12**, 233 (2021).
- [7] J. M. Pino, J. M. Dreiling, C. Figgatt, J. P. Gaebler, S. A. Moses, M. S. Allman, C. H. Baldwin, M. Foss-Feig, D. Hayes, K. Mayer, C. Ryan-Anderson, and B. Neyenhuis, *Nature* **592**, 209 (2021).
- [8] C. H. Baldwin, B. J. Bjork, J. P. Gaebler, D. Hayes, and D. Stack, *Physical Review Research* **2**, 013317 (2020).
- [9] D. D. Hayes, D. Stack, B. Bjork, A. C. Potter, C. H. C. H. Baldwin, and R. P. Stutz, *Physical Review Letters* **124**, 170501 (2020).
- [10] C. H. Baldwin, B. J. Bjork, M. Foss-Feig, J. P. Gaebler, D. Hayes, M. G. Kokish, C. Langer, J. A. Sedlacek, D. Stack, and G. Vittorini, *Physical Review A* **103**, 012603 (2021).
- [11] S. Debnath, *A Programmable Five Qubit Quantum Computer Using Trapped Atomic Ions*, Ph.D. thesis, University of Maryland, College Park, MD (2016).
- [12] J. Preskill, *Proceedings of the Royal Society London A* **454**, 385 (1998).
- [13] E. Knill, *Nature* **463**, 441 (2010).
- [14] T. D. Ladd, F. Jelezko, R. Laflamme, Y. Nakamura, C. Monroe, and J. L. O'Brien, *Nature*



- 464**, 45 (2010).
- [15] A. M. Steane, *Physical Review A* **68**, 042322 (2003).
- [16] J. P. Gaebler, T. R. Tan, Y. Lin, Y. Wan, R. Bowler, A. C. Keith, S. Glancy, K. Coakley, E. Knill, D. Leibfried, and D. J. Wineland, *Phys. Rev. Lett.* **117**, 060505 (2016).
- [17] C. J. Ballance, T. P. Harty, N. M. Linke, M. A. Sepiol, and D. M. Lucas, *Phys. Rev. Lett.* **117**, 060504 (2016).
- [18] Y. Wang, S. Crain, C. Fang, B. Zhang, S. Huang, Q. Liang, P. H. Leung, K. R. Brown, , and J. Kim, *Physical Review Letters* **125**, 150505 (2020).
- [19] K. Mølmer and A. Sørensen, *Phys. Rev. Lett.* **82**, 1835 (1999).
- [20] A. Sørensen and K. Mølmer, *Phys. Rev. A* **62**, 022311 (2000).
- [21] G. Milburn, S. Schneider, and D. James, *Fortschritte der Physik* **48**, 801 (2000), <https://onlinelibrary.wiley.com/doi/pdf/10.1002/1521-3978>.
- [22] M. Mohseni, A. T. Rezakhani, and D. A. Lidar, *Physical Review A* **77**, 032322 (2008).
- [23] R. Blümel, N. Grzesiak, N. Pienti, K. Wright, and Y. Nam, *npj Quantum Information* **7**, 147 (2021).
- [24] Y. Wu, S.-T. Wang, and L.-M. Duan, *Phys. Rev. A* **97**, 062325 (2018).
- [25] A. Sørensen and K. Mølmer, *Physical Review Letters* **82**, 1971 (1999).
- [26] C. F. Roos, *New J. Phys.* **10**, 013002 (2008).
- [27] G. Zarantonello, H. Hahn, J. Morgner, M. Schulte, A. Bautista-Salvador, R. F. Werner, K. Hammerer, and C. Ospelkaus, *Phys. Rev. Lett.* **123**, 260503 (2019).
- [28] P. H. Leung, K. A. Landsman, C. Figgatt, N. M. Linke, C. Monroe, and K. R. Brown, *Phys. Rev. Lett.* **120**, 020501 (2018).
- [29] T. J. Green and M. J. Biercuk, *Phys. Rev. Lett.* **114**, 120502 (2015).
- [30] D. Hayes, S. M. Clark, S. Debnath, D. Hucul, I. V. Inlek, K. W. Lee, Q. Quraishi, and C. Monroe, *Phys. Rev. Lett.* **109**, 020503 (2012).
- [31] A. R. Milne, C. L. Edmunds, C. Hempel, F. Roy, S. Mavadia, and M. J. Biercuk, *Phys. Rev. Applied* **13**, 024022 (2020).
- [32] R. Blümel, N. Grzesiak, N. H. Nguyen, A. M. Green, M. Li, A. Maksymov, N. M. Linke, and N. Yunseong, *Physical Review Letters* **126**, 220503 (2021).
- [33] W. H. Press, S. A. Teukolsky, W. T. Vetterling, and B. P. Flannery, *Numerical Recipes in Fortran 77*, 2nd ed. (Cambridge University Press, Cambridge, 1992).

[34] M. A. Nielsen, *Physics Letters A* **303**, 249 (2002).

[35] S. Blanes, F. Casas, J. A. Oteo, and J. Ros, *Physics Reports* **470**, 151 (2009).